Mouse Ifit1b is a cap1-RNA binding protein which inhibits mouse coronavirus translation and is regulated by complexing with Ifit1c

Harriet V. Mears[1*] and Trevor R. Sweeney[1*]

1 Division of Virology, Department of Pathology, University of Cambridge, Addenbrooke's Hospital, Hills Road, Cambridge, UK.

* Co-corresponding authors: Harriet Mears and Trevor Sweeney
Email: hvm30@cam.ac.uk and ts629@cam.ac.uk

Running Title: Mouse Ifit1b paralogues are functional antiviral effectors.

Keywords: RNA binding protein, mRNA, translation control, innate immunity, viral immunology, mouse, interferon induced proteins with tetratricopeptide repeats (IFIT).

Abstract

Knock-out mouse models have been extensively used to study the antiviral activity of interferon-induced protein with tetratricopeptide repeats (IFIT). Human IFIT1 binds to cap0 (m7GpppN) RNA, which lacks methylation on the first and second cap-proximal nucleotides (cap1, m7GpppNm, and cap2, m7GpppNmNm, respectively). These modifications are signatures of 'self' in higher eukaryotes, while unmodified cap0-RNA is recognised as foreign and, therefore, potentially harmful to the host cell. IFIT1 inhibits translation at the initiation stage by competing with the cap-binding initiation factor complex, eIF4F, restricting infection by certain viruses that possess 'non-self' cap0-mRNAs. However, in mice and other rodents the IFIT1 orthologue has been lost and the closely-related Ifit1b has been duplicated twice, yielding three paralogues: Ifit1, Ifit1b and Ifit1c. While murine Ifit1 is similar to human IFIT1 in its cap0-RNA binding selectivity, the roles of Ifit1b and Ifit1c are unknown. Here, we found that Ifit1b preferentially binds to cap1-RNA, while binding is much weaker to cap0- and cap2-RNA. In murine cells, we show that Ifit1b can modulate host translation and restrict wildtype mouse coronavirus infection. We found that Ifit1c acts as a stimulatory cofactor for both Ifit1 and Ifit1b, promoting their translation inhibition. In this way, Ifit1c acts in an analogous fashion to human IFIT3, which is a cofactor to human IFIT1. This work clarifies similarities and differences between the human and murine IFIT families, to facilitate better design and interpretation of mouse models of human infection, and sheds light on the evolutionary plasticity of the IFIT family.

Introduction

Viruses with capped positive-sense RNA genomes must convincingly mimic host mRNA to avoid recognition by cell-intrinsic defence systems. In eukaryotes, the mRNA cap consists of a guanosine nucleotide covalently linked to the first RNA nucleotide by a 5′-5′ triphosphate bridge (capG, GpppNN), which is methylated at the N-7 position (cap0, m^7GpppNN) to facilitate nuclear export and translation initiation factor recruitment. In higher eukaryotes, including insects and vertebrates, mRNA is further modified by methylation on the 2′-hydroxyl of the first and second cap-proximal nucleotide riboses (cap1, m^7GpppNmN and cap2, m^7GpppNmNm) (1). Coronaviruses, including severe acute respiratory syndrome (SARS)-CoV and the newly-emerged SARS-CoV-2, and mosquito-borne flaviviruses, including dengue virus and Zika virus (ZIKV), encode viral 2′-O-methyltransferases to produce cap1 viral mRNAs (2), which effectively mimic those of the host to avoid immune surveillance.

Sensing of mRNA 2′-O-methylation in vertebrates is primarily mediated by a family of antiviral RNA binding proteins known as interferon-induced proteins with tetratricopeptide repeats (IFIT). In most mammals, including humans, the IFIT family comprises five members: IFIT1, IFIT1B, IFIT2, IFIT3 and IFIT5 (3, 4). IFITs are comprised of tandem tetratricopeptide repeat (TPR) motifs which form superhelical N- and C-terminal domains joined by a pivot domain of variable length and flexibility (5). Structures of human IFIT1 and IFIT5 have shown that the groove between these N- and C-terminal domains is lined with positively charged residues which non-specifically coordinate the phosphate backbone of single-stranded RNA (6–10). As such IFIT5 binds specifically to single-stranded RNA that lacks a 5′ cap (5′ppp) (7, 11, 12). IFIT1 has an additional hydrophobic cavity within the N-terminus which can accommodate the 5′ cap, and consequently has high affinity for cap0 RNA (8). However, due to steric restrictions within the mRNA

binding channel, IFIT1 binds to cap1 RNA with much lower affinity and cannot bind to cap2-RNA (8, 13). Binding to the 5′ extremity of cap0 transcripts allows IFIT1 to effectively out-compete the cap-binding eukaryotic translation initiation factor (eIF) 4F, thereby inhibiting translation at the initiation stage (11). While IFIT3 does not bind RNA directly, its ability to form a complex with IFIT1 via a conserved C-terminal interaction motif greatly increases IFIT1 stability and cap0-RNA binding affinity, thereby promoting IFIT1 antiviral activity (13, 14).

Mouse models have been used extensively to examine the role of IFIT proteins in regulating human disease (see (15)). Like human IFIT1, murine Ifit1 can bind to cap0 RNA with high affinity (16). *In vivo*, mutation of the virally-encoded 2′-O-methyltransferase in a number of flavivirus and coronavirus species severely attenuated viral replication, and vaccination with these viruses can protect mice from challenge with virulent strains (17–22). Virulence was partially or fully restored upon Ifit1 knockout, indicating specific antiviral activity against cap0 viruses (17, 18, 21–23). However, recent phylogenetic analysis has concluded that murine Ifit1 and human IFIT1 are not orthologous and these proteins have different antiviral activity against cap0 and cap1 viruses (4). Indeed, while human IFIT1 can bind to cap1-RNA with low affinity (8, 13), murine Ifit1 lacks any cap1 binding activity (4, 16).

Not only has IFIT1 been lost in mice and related mouse-like rodents, including model organisms such as the Norway rat and Chinese hamster, but IFIT5 is also absent (4). Instead, these species typically harbour multiple copies of the Ifit1b gene. In mice, Ifit1b has been duplicated twice, yielding three paralogues: Ifit1, Ifit1b and Ifit1c (Figure 1A) (also called Ifit1b1, Ifit1b2 and Ifit1b3, to reflect their evolutionary relatedness) (4). Despite the high degree of sequence identity between these paralogues, their functions remain unknown and there is little evidence supporting their expression in mouse cells. In these species, Ifit3 has also undergone a 3′ truncation and lacks the potential to interact with murine Ifit1 (4, 13, 14). Therefore, rodent Ifits may have alternative mechanisms to regulate their expression and function which are distinct from the human IFIT complex.

In this study, we investigated the expression and activity of the entire murine Ifit family. We verified expression of non-canonical family members Ifit1b, Ifit1c and Ifit3b in murine cells, and found that Ifit1b binds to cap1-RNA with remarkable affinity and specificity. Ifit1b selectively inhibited cap1-RNA translation and restricted the replication of wildtype mouse coronavirus *in vitro*. We then established the different Ifit complexes which can form in mice and found that Ifit1c acts as a cofactor to Ifit1 and Ifit1b, promoting their stability and translation inhibition activity, thereby fulfilling a role analogous to human IFIT3. As such, this study helps to elucidate the ways in which primates and rodents have developed convergent roles for IFIT proteins in the innate immune response which occupy their same functional niche. We additionally highlight key distinctions between the human and murine IFIT families, in the hope that this will inform use of mouse models in understanding IFIT biology and antiviral activity.

Results

Ifit1b, Ifit1c and Ifit3b are expressed in murine cells following stimulation

To date, a systematic and quantitative examination of the induction kinetics of the entire murine Ifit family has not been carried out. While the expression patterns of murine Ifit1, Ifit2 and Ifit3 have been examined in detail (24–27), the expression of the other three members of the murine Ifit family, Ifit1b, Ifit1c and Ifit3b, has yet to be formally verified in mouse cells. To address this, murine Ifit expression was examined in RAW264.7 macrophage-like cells, 17Cl-1 immortalised fibroblasts and murine embryonic fibroblasts (MEF). Cells were stimulated with recombinant IFNβ or transfected with synthetic dsRNA (polyI:C) for up to 48 hours. Cell lysates were examined by RT-qPCR and immunoblot analysis, using qPCR primers (Figure S1) and antibodies (Figure S2) specific to each murine Ifit family member. Since Ifit3 and Ifit3b differ by only 5 amino acids, it was not possible to differentiate between these proteins by immunoblotting so, to reflect this, this band will be annotated as Ifit3/3b.

Consistent with previous reports (25, 26), Ifit1, Ifit2 and Ifit3 mRNA expression was rapidly induced following stimulation of RAW264.7 cells, with peak expression observed at 3 to 6 hours post stimulation (Figure 1B, Figure S3A). Expression decreased between 9-24 hours post stimulation. Ifit1, Ifit2 and Ifit3/3b proteins were detectable 6-12 hours following stimulation, just after the peak of mRNA expression (Figure 1D). Ifit mRNA expression was induced to a lesser extent in 17Cl-1 fibroblast cells and expression was delayed compared to expression in RAW264.7 cells, with peak mRNA expression at 12-24 hours post stimulation (Figure 1C, Figure S3B). Similarly, at the protein level, Ifit1, Ifit2 and Ifit3/3b were detectable at 24-48 hours post stimulation (Figure 1E), slightly later than in the RAW264.7 cells. In MEFs, the Ifit mRNA induction patterns were similar to RAW264.7 cells, though the magnitude of induction was 10- to 100-fold lower, and expression had largely returned to baseline by 24 to 48 hours post stimulation (Figure S3C). In both 17Cl-1 cells and MEFs, induction of Ifit2 expression was lower compared to RAW264.7 cells, indicating that Ifit2 may be regulated differently in fibroblasts compared to macrophages (Figure 1-compare D and E, and Figure S3).

mRNA expression was observed for Ifit1b, Ifit1c (Figure 1B,C) and Ifit3b (Figure S3) following stimulation and could be verified by Sanger sequencing of the qPCR product (Figure S1). While Ifit3b expression was strongly induced following stimulation, Ifit1b and Ifit1c were poorly upregulated, with only 10- to 100-fold induction over baseline in all cell lines tested. We tested a number of antibodies to confirm Ifit expression at the protein level. A commercially available antibody against human IFIT1 was cross-reactive with murine Ifit1, but detected Ifit1b to a greater extent (Figure S2B). This antibody could detect a signal in IFN-stimulated mouse cells, but since it reacted with both Ifit1 and Ifit1b, the identity of this signal was ambiguous. A peptide-raised antibody against Ifit1b detected Ifit1b without cross-reactivity with Ifit1 (Figure S2A) with greater sensitivity (Figure S2C). Using this antibody, in 17Cl-1 cell lysates, Ifit1b was detectable at the protein level 48 hours (Figure 1E) and 80 hours (Figure S2D) post IFN stimulation. A peptide-raised antibody against Ifit1c was highly specific for recombinant Ifit1c protein but could not reproducibly detect endogenous Ifit1c in stimulated mouse cells (Figure S2A).

To investigate the reason behind the poor expression of Ifit1b and Ifit1c in murine cells, the promoter regions of Ifit1, Ifit1b and Ifit1c were examined. Ifit1 has two well-defined tandem interferon stimulated response elements (ISRE) within 100bp of the transcription start site (TSS) (Figure S4A). The Ifit1c promoter region contains one canonical ISRE sequence proximal to the TSS, and a second ISRE-like sequence further upstream. For Ifit1b, there are two annotated TSS: one proximal to the coding sequence of Ifit1b (here designated Ifit1b_1) and one several kilobases upstream (Ifit1b_2), which overlaps the Ifit1 promoter region (Figure 1A), both of which contain poorly-conserved ISRE-like sequences (Figure S4A).

Promoter plasmids were designed to express firefly luciferase (Fluc) under the control of the murine Ifit promoters. The promoter sequence was defined as 0.8-1 kb upstream of the transcription start site (TSS) for each Ifit gene. A control plasmid was also generated with 1 kb of scrambled DNA sequence upstream of the Fluc mRNA (SCR). Promoter plasmids were co-transfected into 17Cl-1 cells alongside a constitutive Renilla luciferase (Rluc) expression plasmid. After 4 hours, cells were treated with IFNβ to stimulate promoter activity, then harvested after 24 hours to determine luciferase expression. Luciferase activity was normalised to the Rluc control for each condition.

As expected, luciferase production from the Ifit1 promoter was strongly stimulated by treatment with IFNβ (Figure S4B). For Ifit1b, the upstream Ifit1b_2 promoter weakly drove Fluc expression but was not IFN responsive, while the downstream Ifit1b_1 promoter was slightly stimulated in response to IFNβ. Similarly, the Ifit1c promoter showed a small degree of upregulation when cells were treated with IFNβ (Figure S4B). Therefore, the lower expression of Ifit1b and Ifit1c at the mRNA level, described above, may be due to poorly IFN-responsive promoter sequences.

Ifit1b specifically inhibits translation of cap1 mRNA.

We next sought to examine the effect of the murine Ifit proteins on translation, using an *in vitro* translation assay system, which we have previously used to examine the effect of human IFIT heterocomplexing on their function (14). An Fluc reporter mRNA flanked by the 5′ and 3′ untranslated regions of human β-globin (Globin-Fluc) was transcribed and capped *in vitro* (Figure 2A,B). The efficiency of cap methylation was verified using a primer extension inhibition assay, based on the propensity of reverse transcriptase to terminate at methylated nucleotides, dependent on Mg^{2+} concentration (28, 29). Reverse transcription was carried out using AMV reverse transcriptase in the presence of a range of Mg^{2+} concentrations. At high Mg^{2+} concentrations, full-length signal was present for all mRNAs, as well as a proportion of 1 nt longer cDNAs, consistent with low-level terminal transferase activity (29). At lower Mg^{2+} concentrations however, 1 or 2 nt shorter cDNA products were predominant for cap1 and cap2 RNA, respectively. At very low Mg^{2+} concentrations, only the lower band was detectable for cap1 and cap2 RNA, but not for cap0 RNA. This indicates high cap methylation efficiency, since no residual full-length signal was detectable (Figure 2B).

Murine Ifit proteins were expressed and purified as described in the Materials and Methods, with the exception of Ifit1c, which was poorly expressed and insoluble *in vitro*. Ifit proteins were normalised by western blotting against the C-terminal His_8-tag (Figure 2C). Globin-Fluc reporter mRNAs were incubated with 500 nM recombinant Ifit protein before the addition of RRL and translation was quantified by

measuring luminescence from the Fluc reporter, normalised to the buffer only control. Consistent with previous reports (4, 13, 16), Ifit1 strongly inhibited translation of the cap0 reporter, but could not inhibit cap1 or cap2 translation (Figure 2D). Translation from the uncapped reporter mRNA was much less efficient than any of the capped RNAs but was not reproducibly inhibited by any Ifit protein tested (Figure 2D, left panel). Ifit2, Ifit3 and Ifit3b did not inhibit translation of any of the RNAs tested, consistent with the described activities of human IFIT2 and IFIT3 (5, 11, 12). However, Ifit1b strongly inhibited the translation of cap1 Globin-Fluc RNA, but had no effect on cap0- or cap2-RNA translation (Figure 2D).

Ifit1b inhibits wildtype mouse coronavirus translation

To investigate Ifit1b cap1-RNA translation inhibition in more detail, titration experiments were performed using the Globin-Fluc reporter, or reporters with viral 5′ and 3′UTRs flanking the same Fluc ORF (Figure 3A). Representative species of coronavirus (mouse hepatitis virus, MHV) and flavivirus (ZIKV) were chosen, which have different degrees of RNA secondary structure at their 5′ ends (Figure S5). Serial dilutions of Ifit1b were incubated with Fluc mRNAs bearing differentially methylated 5′ caps, and luciferase activity was used to monitor translation in RRL, as previously. 50% inhibitory concentrations were interpolated from the data and are presented in Table 1. Consistent with its described cap0-RNA binding activity, Ifit1 caused a dose-dependent inhibition of cap0 globin-Fluc mRNA translation (IC_{50} = 102 nM, Figure 3B, dotted line). Ifit1b inhibited cap1 Globin-Fluc translation at low concentrations, comparable to inhibition of cap0 mRNA by Ifit1 (IC_{50} = 152 nM, Figure 3B, red line). However, even at the highest concentrations of Ifit1b tested, there was still a low level of cap1-RNA translation, compared to complete inhibition of cap0-RNA translation by Ifit1. Ifit1b only weakly inhibited cap0 and cap2 Globin-Fluc translation (IC_{50} ~ 675 nM and ~ 825 nM, respectively).

MHV-Fluc mRNA was slightly more susceptible to translation inhibition by Ifit proteins. Ifit1 inhibited the translation of cap0-MHV-Fluc RNA at 1.6-fold lower concentrations compared to inhibition of cap0-Globin-Fluc (IC_{50} = 68 nM, Figure 3C, dotted line). Likewise, Ifit1b inhibited the translation of cap1-MHV-Fluc RNA at 1.5-fold lower concentrations compared to cap1-Globin-Fluc RNA (IC_{50} = 101 nM, Figure 3C, red line). Inhibition of the cap0-MHV reporter by Ifit1b was similar to the inhibition of the cap0-Globin reporter (IC_{50} ~ 690 nM), supporting specificity for cap1-RNA binding over cap0. However, inhibition of cap2-MHV mRNA was slightly greater, indicating looser binding specificity to this reporter (IC_{50} = 238 nM). Therefore, the sequence or structure of MHV mRNA may alter cap-binding specificity, as well as affinity.

By contrast, ZIKV-Fluc mRNA translation was resistant to both Ifit1 and Ifit1b, even at micromolar concentrations (Figure 3D). At the highest concentrations of Ifit1 or Ifit1b tested, ZIKV-Fluc translation was inhibited by a maximum of 30-50% by either Ifit1 or Ifit1b. We have previously shown that human IFIT1 could completely inhibit the translation of the same cap0 ZIKV-Fluc reporter at nanomolar concentrations, and could inhibit cap1 ZIKV-Fluc translation at micromolar concentrations (14). Therefore, the inability of murine Ifit proteins to inhibit the translation of the same reporter mRNA is quite surprising.

Since Ifit1b could strongly inhibit the translation of cap1 MHV-Fluc reporter mRNAs, we reasoned that Ifit1b may be capable of inhibiting the lifecycle of ('restricting') MHV in cell culture. To investigate this, plasmids encoding mCherry-tagged Ifit1, eGFP-tagged Ifit1b or eGFP alone were electroporated into 17Cl-1 mouse fibroblast cells, which are permissive for MHV infection (30). After 24 hours, cells were infected with wildtype MHV strain A59 (genome structure shown in Figure 4A, upper panel) at an MOI of 0.05 pfu/cell. After 16 hours, cells were harvested for immunofluorescence or flow cytometry analysis (experimental timeline shown in Figure 4A, lower panel).

Cells on coverslips were fixed and stained for double-stranded RNA, a well-described marker for RNA virus replication complexes (31). In empty vector or eGFP-transfected cells, 14 hours after infection with MHV the majority of cells showed dsRNA staining in the cytoplasm, while dsRNA was not visible in uninfected cells (Figure 4B). eGFP-expressing cells were positive for dsRNA, indicating that overexpression of eGFP had no effect on viral replication. Similarly, many mCherry-Ifit1 expressing cells were also positive for dsRNA signal, indicating that Ifit1 is not directly antiviral (Figure 4B, white arrowheads), though the dsRNA signal appeared to be lower in the cell population. By contrast, few cells overexpressing eGFP-Ifit1b were positive for dsRNA, implying a direct antiviral effect of Ifit1b on coronavirus infection (Figure 4B, open arrowheads).

To quantify restriction by Ifit1b, 17Cl-1 cells were electroporated with Ifit expression plasmids and infected with MHV, as previously, then fixed in suspension and stained for dsRNA, before analysis by flow cytometry (see Figure S6). Before infection, fluorescent protein expression was checked by microscopy at 20 hours post electroporation and transfection efficiency was comparable between plasmids (Figure S6A). The eGFP-Ifit1b-transfected cell population had much lower dsRNA signal compared to empty vector or eGFP-transfected cells, indicating that it was resistant to infection with MHV (Figure 4C). Importantly, cells transfected with a mutant of Ifit1b which does not bind to cap1-RNA (Ifit1b-WM, described further in Figure 6) were infected to the same extent as eGFP- or empty vector-transfected cells, indicating that Ifit1b restricts MHV infection in a manner dependent on its RNA-binding activity. eGFP-Ifit1b and eGFP-Ifit1b-WM expression was equivalent when analysed by flow cytometry (Figure S6C). Therefore, these data support an antiviral role for Ifit1b in MHV infection and correlates with an inhibition of viral translation by binding to the cap1-RNA genome.

By contrast, infection of mCherry-Ifit1-transfected cells was similar to infection of empty vector-transfected cells, indicating that Ifit1 does not inhibit MHV infection in these cells (Figure S6E). This is consistent with the inability of Ifit1 to bind to cap1-RNA. However, we have previously observed that murine Ifit1 may promote type I IFN expression in mouse cells and thereby restrict mouse norovirus infection (32). Since 17Cl-1 cells respond slowly to dsRNA (see Figure 1) and do not upregulate ISG expression during acute MHV infection (33), this may explain why we did not observe an antiviral phenotype for Ifit1 in this cell type.

Ifit1b regulates host translation

It has been estimated that between 30-70% of mouse mRNA transcripts have cap1 5′ ends, with the remainder bearing cap2 (34), while cap0 5′ ends are undetectable in various human and mouse cells (35). Therefore, we hypothesised Ifit1b should be capable of inhibiting the translation of a proportion of host mRNA transcripts. To investigate this, a puromycylation labelling approach was taken (36). Puromycin is an antibiotic which mimics the structure of aminoacylated tRNA and is thus incorporated into the nascent polypeptide chain during elongation, resulting in premature chain termination. When mammalian cells are treated with low concentrations of puromycin, it is stochastically incorporated towards the C-termini of nascent polypeptides. Using antibodies raised against puromycin, these labelled proteins can be detected by western blotting, thereby allowing visualisation of the nascent proteome of the treated cell.

Murine 17Cl-1 fibroblast cells were transfected with FLAG-tagged Ifit1 or Ifit1b for 16 hours before treatment with 5 μg/mL puromycin for a further 4 hours. Cell lysates were separated by SDS-PAGE and transferred to nitrocellulose membranes, which were stained with REVERT total protein stain to ensure an equal quantity of lysate was loaded in each well (Figure S7). Membranes were then analysed by immunoblotting, using a monoclonal antibody against puromycin. Cells overexpressing Ifit1b showed a 30% reduction in puromycin incorporation, compared to the empty vector control, indicating that Ifit1b can indeed inhibit a proportion of cellular translation (Figure S7). Cells overexpressing Ifit1 showed similar levels of incorporation to empty vector-transfected cells, indicating little effect on cellular translation.

Ifit1b binds specifically to cap1 RNA.

Ifit1b has previously been hypothesised not to bind to RNA since it has residues in the cap-binding pocket and RNA-binding channel which could disrupt association with RNA, based on structural and mutational analysis of human IFIT1 (8). Therefore, we wanted to determine whether inhibition of cap1 translation by Ifit1b was due to RNA binding or a different mode of action. Previously, we have used a primer extension inhibition approach to determine the RNA binding affinity of IFIT proteins. However, unlike Ifit1, Ifit1b-RNA binding could not be visualised by primer extension (Figure S8).

As an alternative approach, a thermal stability assay was developed to examine Ifit1b-RNA binding. This technique employs a dye which fluoresces when it binds to hydrophobic patches exposed as a protein unfolds, to quantify protein melting temperature (37). Binding to a substrate can increase the thermal stability of proteins, resulting in an increase in a melting temperature which correlates with its binding kinetics (38). Since it is known that IFIT proteins adopt more stable ‘closed’ conformations upon RNA binding (7), we reasoned that RNA binding should stabilise Ifit melting temperature.

Ifit proteins were melted in the presence of increasing concentrations of an RNA oligonucleotide, comprising the first 25 nucleotides of the human **β**-globin 5′UTR (globin25), which is predicted to be unstructured (Figure 5A). A short oligonucleotide was chosen to minimise nonspecific stabilisation, for example resulting from interactions between the body of the RNA and the surface of the Ifit protein. Globin25 oligonucleotides were purified by size exclusion chromatography to remove small molecule

contaminants and capping efficiency was confirmed by high resolution denaturing PAGE (Figure 5B). Since both specific and non-specific binding can contribute to protein stabilisation, heterologous yeast tRNA was included as a blocking agent, such that only specific, high-affinity interactions which are sufficient to displace bound tRNA produce a signal above baseline.

Increasing concentrations of cap0 RNA resulted in a dose-dependent stabilisation of Ifit1, as expected (Figure 5C). Cap1 RNA did not stabilise Ifit1, but actually slightly reduced Ifit1 melting temperature (Figure 5C). Consistent with the translation inhibition assays, Ifit1b was stabilised in a dose-dependent manner by cap1-globin25 RNA, indicative of binding (Figure 5D). Stabilisation by cap0-globin25 RNA was lower, supporting specific binding to cap1-RNA over cap0-RNA.

To investigate the mechanism of RNA binding by Ifit1b, we generated a panel of point mutants based on homology modelling (see Methods) with the human IFIT1/cap0 RNA structure (Figure 6A). The mutant proteins were purified and normalised by immunoblotting against the C-terminal His8 tag (Figure 6B). These were then incubated with a two-fold molar excess of cap0- or cap1-globin25 RNA, before thermal stability analysis. Mutation of a conserved tryptophan residue, W152, which is necessary for cap guanosine coordination by human IFIT1 (8), reduced stabilisation of Ifit1b by cap1-RNA back to background levels (Figure 6C). Mutation of the charged residues in the cap-binding loop had little effect on cap1-RNA binding. Mutation of E50 to alanine or glutamine only slightly reduced cap1 RNA binding, while mutation of R54 to alanine or leucine reduced stabilisation by cap1 RNA by about half. Mutation of both E50 and R54 to the equivalent residues in Ifit1, and conserved in human IFIT1 (glutamine and leucine, respectively), restored cap1 binding back to wildtype levels (Figure 6C). Previously, in human IFIT1, mutation of these residues to alanine only slightly reduced cap0-RNA binding (8), indicating that they contribute to stable cap binding but their exact identity is not critical. We also observed a slight increase in cap0-RNA binding by the E50A and E50Q/R54L mutants, indicating they may impact RNA binding specificity, even though these residues do not contact the first RNA nucleotide (Figure 6D, left panel). Together this indicates that Ifit1b likely engages the cap using the conserved tryptophan-144 residue but the other face of the cap-guanosine is coordinated non-specifically, in this case by long, polar side-chains in the cap-binding loop, which may impact cap-binding specificity.

Next, mutations were made within the RNA binding channel to investigate how Ifit1b achieves specific cap1 RNA binding. In human IFIT1, the residues immediately proximate to the ribose 2′-hydroxyl group, Y157 and R187, sterically hinder binding to 2′-O-methylated RNA (8) (Figure 6D, right panel). In murine Ifit1b the tyrosine is conserved at position 162, but the arginine residue is substituted for H192. Therefore, H192 was investigated for its contribution to RNA methylation sensing, by mutation to alanine, arginine or glutamate. Mutation to alanine reduced stabilisation by cap1 RNA by half, while mutation to glutamate had no effect on cap1-RNA binding. However, H192E increased stabilisation of Ifit1b by cap0 RNA by two-fold, indicating that H192 may indeed play a role in discriminating RNA methylation state (Figure 6C. Mutation of H192 to arginine, mimicking human IFIT1 and murine Ifit1, abrogated RNA binding entirely. However, Ifit1b H192R was less stable than wildtype Ifit1b, indicating that H192R may disrupt the correct folding of Ifit1b, accounting for the loss of RNA binding activity. The reciprocal in human IFIT1 (R187H) similarly abolished cap0-RNA binding (8).

Murine Ifit proteins form heterodimeric complexes.

We and others recently reported that the interaction between human IFIT1 and IFIT3 is important for regulation of IFIT1 activity (13–15). However, murine Ifit3 cannot interact with murine Ifit1 (13, 16), due to a genetic truncation in mouse-like rodents, which deletes the region of the protein responsible for IFIT1 interaction (Figure S9). However, the C-terminal YxxxL motif, critical for human IFIT1-IFIT3 complex formation, is conserved in murine Ifit1, Ifit1b and Ifit1c, indicating that these proteins may be capable of hetero-complexing (Figure 7A, S10).

We first examined the oligomeric state of Ifit proteins in solution. Human IFIT1 was recently described to homodimerise in a concentration-dependent manner, via the C-terminal YxxxL motif (39). BSA, which is a 65 kDa monomer with a small proportion of 132 kDa dimeric species, was used as a size marker for size exclusion chromatography (SEC). When analysed by SEC, Ifit1 and Ifit1b eluted after the BSA dimer but before the BSA monomer peak, indicating that these proteins are homodimers (Figure S11A,B). This was confirmed for Ifit1b, which had the molecular weight of a dimer when analysed by SEC coupled with multi-angle light scattering (SEC-MALS) at different concentrations (Figure S11C). When the YxxxL motif was mutated in either Ifit1 or Ifit1b, the mutant proteins eluted later on the SEC column, after the BSA monomer, indicating that they are indeed monomeric (Figure S11A,B). When analysed by SEC, MBP-Ifit1c$_{CTD}$ eluted in the void fraction, consistent with the poor stability of this protein and its tendency to aggregate, and so was not suitable for SEC-MALS analysis.

To investigate which murine Ifit proteins can interact with each other, an *in vitro* co-precipitation assay was used, similar to that employed by Johnson et al *(2018)* for the interrogation of human IFIT interactions. Equimolar MBP-tagged bait and His-tagged prey proteins were incubated together at 30˚C for one hour, before precipitation on amylose resin. Ifit3 was included as a negative control in each experiment and, consistent with a recent report (13), did not co-precipitate with any of the baits tested (Figure 7B-D). MBP-Ifit1 precipitated both Ifit1b and Ifit1 (Figure 7B and S12A), while MBP-Ifit1b precipitated both Ifit1 and Ifit1b (Figure 7C, Figure S12B), indicating that Ifit1 and Ifit1b are capable of heterocomplexing. When Ifit1 and Ifit1b were incubated together and analysed by SEC, the eluting species was the same size as the Ifit1 or Ifit1b homodimers, and higher order species were not detected (Figure S11D). MBP alone did not interact with Ifit1b or Ifit3 (Figure 7B, lower panel), but pulled down a trace amount of Ifit1 (Figure 7C, lower panel). Since Ifit1 had a tendency to precipitate during this assay, this likely represents nonspecific binding of Ifit1 to the MBP or to the beads themselves.

To determine whether Ifit1 or Ifit1b could interact with Ifit1c, full-length MBP-tagged Ifit1c was used as bait. Recombinant full-length Ifit1c was highly unstable and, despite exhaustive efforts, refractory to purification. MBP-tagged Ifit1c was soluble but was nevertheless highly impure (Figure S12C,D). However, despite the contaminants present in the recombinant MBP-Ifit1c, Ifit1b was clearly visible in the precipitate, indicative of an interaction (Figure S12D). Owing to the presence of a contaminant band in Ifit1c at the same molecular weight as Ifit1, this interaction was more difficult to confirm (Figure 12C). To circumvent this, a truncated MBP-tagged Ifit1c construct was generated, containing the three most C-

terminal TPRs (MBP-Ifit1c$_{CTD}$, amino acids 338-470, Figure S12E), which allowed purification of clean recombinant Ifit1c for use as bait. Ifit1 and Ifit1b both precipitated with MBP-Ifit1c$_{CTD}$, while Ifit3 did not (Figure 7D). Therefore, Ifit1c can specifically form complexes with both Ifit1 and Ifit1b via its C-terminal domain.

The relative affinity of these interactions was investigated by competitive co-precipitation experiments. MBP-tagged Ifits were used as bait, and incubated with prey protein at 30 ˚C before binding to amylose resin, as previously. Beads were then washed with increasing concentrations of a competitor prey protein, with the expectation that higher affinity interactions should displace lower affinity ones. However, we observed that even high concentrations of Ifit1b could not disrupt the interaction between Ifit1 and MBP-Ifit1c$_{CTD}$ (Figure S12F), and likewise Ifit1 did not disrupt the Ifit1b-MBP-Ifit1c$_{CTD}$ complex (Figure S12G). Next, MBP-Ifit1c$_{CTD}$ was incubated together with both Ifit1 and Ifit1b, at different temperatures. When incubated together on ice MBP-Ifit1c$_{CTD}$ coprecipitated both Ifit1 and Ifit1b, to a similar extent (Figure S12H). Since this interaction occurred even at low temperatures, it indicates that heterocomplexing is preferential and high affinity, but Ifit1c binds to both Ifit1 and Ifit1b with comparable affinity. Slightly more Ifit1 coprecipitated with MBP-Ifit1c$_{CTD}$ when the proteins were incubated at 30 ˚C (Figure S12I), which may be indicative of aggregation, rather than true preferential interaction, as we observed with MBP-only (see Figure 7C, lower panel). Therefore, these experiments indicate that purified Ifit1c can interact with both Ifit1 and Ifit1b to a similar extent, and these interactions are preferential over homodimerisation.

Heterocomplexing enhances Ifit stability *in vitro*.

We previously observed that functionally important human IFIT heterocomplexes were more stable than IFIT proteins in isolation, both *in vitro* and in human cells (14). Therefore, we analysed the thermal stability of murine Ifit proteins and complexes using differential scanning fluorimetry. Ifit proteins were incubated alone or in combination for 30 minutes on ice, then assayed for thermal stability, as described above for the Ifit1b RNA binding assay. Full length Ifit1c could not be used due to the high degree of contaminants present, so instead the C-terminal fragment of Ifit1c was analysed. Ifit1c$_{CTD}$ was expressed without an MBP tag, since MBP is very stable and would interfere with the melt curve analysis.

Murine Ifit1 and Ifit1b alone were relatively unstable, with melting temperatures around physiological temperature (Figure 7E, Table 2). For comparison, MBP had a melting temperature of 60 °C when analysed under the same conditions (Figure 7E, dashed line). When Ifit1 and Ifit1b were mixed together, the melt curve was intermediate between the melting temperatures of the constituent proteins, indicating that this interaction does not provide any stability to either protein (Figure 7E). Ifit1c$_{CTD}$ alone was very unstable and did not produce a quantifiable melt curve. However, when either Ifit1 or Ifit1b was mixed with increasing concentrations of Ifit1c$_{CTD}$, melting temperature increased by up to 3 ˚C (Figure 7F,G Table 2). Therefore, interaction with the C-terminal domain of Ifit1c enhances the thermal stability of both Ifit1 and Ifit1b.

Ifit1 and Ifit1b stabilise Ifit1c expression in murine cells.

Ifit heterocomplexes were then examined in mouse cells, to determine if co-expression of different murine Ifit proteins can stabilise their expression. To do this, plasmids were generated which expressed mCherry-tagged Ifit1 or eGFP-tagged Ifit1b, followed by FLAG-tagged Ifit1c in the same open reading frame, separated by the 2A stop-go peptide sequence from thosea asigna virus. The 2A sequence efficiently skips a peptide bond during translation elongation, effectively cleaving the two proteins (40), allowing stoichiometric coexpression of Ifit proteins from the same plasmid. Ifit1c was either wildtype or had a mutant YxxxL (YL) motif to disrupt heterocomplexing. For consistency and clarity, in Figure 8 both mCherry-Ifit1 and eGFP-Ifit1b fluorescent proteins (FP) are shown in green, while FLAG-Ifit1c is shown in magenta (Figure 8A).

Murine 17Cl-1 cells were seeded onto coverslips, then transfected with Ifit co-expression plasmids. After 24 hours, cells on coverslips were fixed and stained for FLAG, while surrounding cells from the same well were harvested for western blotting. When transfected alone, FLAG-Ifit1c expression was very low (Figure 8B,C). However, FLAG-Ifit1c expression was moderately enhanced when co-expressed with mCherry-Ifit1 (Figure 8B) and strongly enhanced by co-expression with eGFP-Ifit1b (Figure 8C). However, when the YxxxL motif in Ifit1c was mutated, expression was similar to Ifit1c alone (Figure 8B,C), indicating that interaction with Ifit1 or Ifit1b is necessary for Ifit1c stabilisation. Neither mCherry-Ifit1 nor eGFP-Ifit1b expression was affected by co-expression with wildtype or mutant Ifit1c (Figure 8B,C).

When analysed by microscopy, mCherry-Ifit1 or eGFP-Ifit1b expressed alone showed diffuse cytoplasmic localisation (Figure 8D,E, left-most panels), typical of IFIT proteins (41, 42). However, when FLAG-Ifit1c was expressed alone, it showed punctate staining within the cytoplasm, with few cells showing diffuse localisation (Figure 8D, top-right panel). These puncta did not significantly colocalise with a proteasome marker and did not aggregate at the proteasome when cells were treated with the proteasome inhibitor MG-132 (Figure S13A). FLAG-Ifit1c expression was also not rescued upon MG-132 treatment (Figure S13B).

When wildtype FLAG-Ifit1c was co-expressed with either mCherry-Ifit1 or eGFP-Ifit1b, both proteins localised in the cytoplasm and very few cells showed punctate staining for Ifit1c (Figure 8D, centre bottom and 8E, centre). Ifit1c expression also appeared to be higher, evident from the brighter fluorescence signal, consistent with the western blotting data (compare Figure 7D, top right to 7D centre bottom). When FLAG-Ifit1c-YL was co-expressed with mCherry-Ifit1 or eGFP-Ifit1b, cells still expressed both signals in the cytoplasm. However, co-localisation of the two signals was not as consistent as for wildtype Ifit1c and many cells still showed punctate FLAG staining (Figure 7D, right bottom and 7E, right). The fluorescence signal was also weaker for FLAG in these cells, indicating lower Ifit1c expression. Therefore, interaction between Ifit1 or Ifit1b and Ifit1c may relocalise Ifit1c within the cytoplasm and stabilise its expression.

The C-terminal domain of Ifit1c stimulates translation inhibition by Ifit1 and Ifit1b.

Next, we sought to determine whether Ifit1c could act as a cofactor for Ifit1 or Ifit1b, by determining translation inhibition activity of Ifit complexes *in vitro*. Increasing concentrations of Ifit1 or Ifit1b were

incubated with cap0 or cap1 MHV-Fluc reporter mRNAs (Figure 9A), in a reaction containing RRL with or without the addition of 500 nM MBP-Ifit1c$_{CTD}$. Luciferase signal was measured, as previously, and normalised to the buffer-only or MBP-Ifit1c$_{CTD}$-only condition for each titration series. IC_{50} values from these experiments are given in Table 3.

Inclusion of MBP-Ifit1c$_{CTD}$ in the translation reaction decreased the concentration of Ifit1 required to cause a 50% decrease in translation from cap0 MHV-Fluc reporter mRNA by 5-fold (Figure 9B). Similarly, addition of MBP-Ifit1c$_{CTD}$ decreased the IC_{50} of Ifit1b on cap1 MHV-Fluc mRNA by 5-fold (Figure 9C). MBP-Ifit1c$_{CTD}$ also enhanced translation inhibition by Ifit1b at higher concentrations, allowing almost complete inhibition of translation, suggesting that Ifit1c may promote saturation of RNA binding by Ifit1b. Addition of mutant MBP-Ifit1c$_{CTD}$-YL did not enhance translation inhibition, indicating that interaction between Ifit1 or Ifit1b and Ifit1c is necessary for Ifit1c cofactor activity (Figure 9B,C). When human IFIT3 was added to a translation reaction with human IFIT1, inhibition of cap0-MHV-Fluc translation was enhanced, as we previously described (14). By comparison, addition of Ifit1c$_{CTD}$ did not affect translation inhibition by human IFIT1 (Figure 9D). Together this indicates that Ifit1c can specifically act as a cofactor for both Ifit1 and Ifit1b to enhance their translation inhibition activity.

Discussion

IFIT proteins play extensive and diverse roles not only in antiviral defence, but also in inflammation, cancer and autoimmunity (reviewed in (15, 43, 44)). Studying their function *in vivo* is invaluable for properly understanding their role in modulating such complex diseases. Given the widespread use of animal models, particularly mice, in biomedical research, it is important to understand how their innate immune systems differ to that of humans in order to properly evaluate the usefulness of data generated by animal studies with regards to human disease. However, in recent years it has become increasingly clear that the human and murine IFIT families differ in key aspects both in terms of their function and their regulation.

Human IFIT1 is well characterised to bind to cap0-RNA *in vitro* and inhibit its translation (8, 11, 16). As such, human IFIT1 can restrict viruses which produce cap0 mRNA, such as those with mutated 2′-O-methyltransferase enzymes (21–23). These viruses are typically attenuated in mouse infection models, and in some cases can be partially or fully restored upon knockout of murine Ifit1 (17, 18, 21–23). Human IFIT1 was more recently shown to bind weakly to cap1-RNA and inhibit its translation at high IFIT1 concentrations. As such, human IFIT1 is capable of restricting the replication of viruses with cap1-RNA when expressed at high levels (4, 13). Murine Ifit1, however, does not share this function and can only inhibit cap0-RNA translation (4, 16), a finding which was recapitulated here.

Instead, we found that a related protein, murine Ifit1b, could inhibit the translation of cap1-RNA at nanomolar concentrations but failed to inhibit cap0 or cap2 translation. We show that overexpression of Ifit1b can inhibit the translation of mouse coronavirus model RNAs, while restricting viral replication in murine cells. Previously, overexpression of murine Ifit2 was shown to slightly inhibit the replication of both WT and cap0-mutant MHV (17), while Ifit2 knockout increased replication of neurotropic MHV and exacerbated viral encephalitis (45). The antiviral effect of Ifit2, however, was due to an enhancement of

innate immune signalling, much like we reported recently for murine Ifit1 (32), rather than a direct effect on viral replication. Human IFIT1 can inhibit cap0-mutant strains of a number of human coronaviruses, while murine Ifit1 can inhibit cap0-mutant MHV, but neither could inhibit the replication of wildtype virus (21–23).

This ability of Ifit1b to specifically sense cap1 methylation is quite striking. Previously, IFIT proteins have been identified which can bind to cap1-RNA with low affinity, particularly rabbit IFIT1B, but in all cases could also bind strongly to cap0-RNA (4, 8, 9, 11). Our mutational analysis implicated histidine-192 as a key residue in Ifit1b cap1 sensing, though the exact mechanism of cap1 discrimination remains uncertain. It is possible that specific contacts are made between H192 and the RNA 2′-O-methyl group itself, to stabilise the Ifit1b-RNA complex, allowing preferential binding to cap1 over cap0. This mechanism of RNA-binding has been shown previously for eIF4E5, one isoform of the cap-binding translation initiation factor eIF4E, from trypanosome parasites. eIF4E5 interacts with cap4-methylated mRNA, a methylation state unique to these parasites, by making specific contacts between certain hydrophobic sidechains and the methylated RNA backbone, resulting in significantly higher affinity of eIF4E5 for cap4- over cap0-RNA (46).

While the translation of unstructured RNAs was efficiently inhibited by murine Ifit1 and Ifit1b, here it was found that neither protein was capable of inhibiting the translation of a ZIKV reporter mRNA, even at micromolar concentrations. Previously we showed that human IFIT1 effectively inhibited translation of the same ZIKV reporter construct at nanomolar concentrations (14), indicating a fundamental difference in the ability of human IFIT and murine Ifit proteins to bind to the same substrate. It was previously shown that alphaviruses have a very stable stem loop at the immediate 5′ end of the genome, which prevents binding by mouse Ifit1 and confers resistance to type I IFN in vivo (47, 48). Destabilising this RNA secondary structure confers susceptibility to restriction by Ifit1 (47). Flaviviruses, including ZIKV, have a comparable stable stem loop at the very 5′ end of their genomes (49) (Figure S5), indicating that they, too, may be refractory to binding by murine Ifit proteins for the same reason.

Such differences in the ability of human IFIT1 and murine Ifits to bind RNA with strong 5′ structure may have implications for vaccine development. In a mouse model of West Nile virus (WNV) infection, a *Flavivirus* closely related to ZIKV, Ifit1 knockout did not restore attenuation of a cap0-mutant WNV strain in some tissues and in primary cultures derived from Ifit1 knockout mice (18). Furthermore, even though Ifit1 is expressed throughout the brain following WNV infection (50), WNV infection in the central nervous system was unaffected by Ifit1 knockout (18). However, both murine Ifit1 and human IFIT1 can restrict cap0-mutant WNV replication in certain cell lines (13, 17, 18) Differences in the expression or activity of IFIT proteins in different tissues between humans and mice may have major implications for the safety and efficacy of a cap0 WNV vaccine strain.

Recently, we and others described a functional complex between IFIT1 and IFIT3 in humans, in which IFIT3 acts as a cofactor to stabilise IFIT1 expression and enhance its RNA binding activity (13, 14). However, in murid rodents, Ifit3 is truncated and lacks the C-terminal domain containing the YxxxL IFIT1 interaction motif and thus cannot interact with Ifit1 (13) (see Figure S9), a finding that was recapitulated

here. However, murine Ifit1, Ifit1b and Ifit1c maintain the YxxxL motif at the C-terminus and we found that these proteins can interact, likely as heterodimers. Like human IFIT complexes, interaction between murine Ifit proteins was shown to increase their thermal stability, suggesting heterocomplexing is a thermodynamically preferable state. In mouse cells, Ifit1c expression was significantly enhanced by co-expression with Ifit1 or Ifit1b. *In vitro*, the C-terminal domain of Ifit1c was sufficient to enhance translation inhibition by Ifit1 and Ifit1b, similar to the enhancement we observed previously for the human IFIT1:IFIT3 complex (14).

The mechanism by which IFIT cofactors enhance translation inhibition remains to be determined. We previously hypothesised that the long C-terminal domain of human IFIT3, which is extended by two a-helices relative to IFIT1, promoted RNA binding by IFIT1 (14). IFIT3 was shown to make contacts with the C-terminal and pivot domains of IFIT1 (13), which suggested that IFIT3 may alter the flexibility of IFIT1, causing it to remain bound to cap0-RNA and thereby increasing its affinity. This, in turn, allows IFIT1 to more effectively out-compete eIF4E for binding to the mRNA cap, inhibiting translation initiation at lower IFIT concentrations. However in mice, Ifit1c does not have a long C-terminal tail which would allow an analogous mechanism of action, suggesting that Ifit1c may act in a different way to enhance RNA binding by Ifit1 and Ifit1b. This may explain why murine Ifit1c could not enhance translation inhibition by human IFIT1, and why human IFIT3 did not bind to murine Ifit1 in a previous study (13).

The YxxxL interaction motif is almost universally conserved in mammalian IFIT1, IFIT1B and, where applicable, IFIT3 protein sequences (see Figure S10). Given that IFIT1 and IFIT1B are cap-RNA binding proteins, this proposes a situation in which the IFIT proteins which are capable of binding to capped RNA need to form complexes with regulatory IFIT cofactors. This may allow fine-tuned expression of IFIT proteins which have the potential to inhibit cellular translation (51), and therefore pose a cytotoxic risk. It may also be a way of integrating IFIT-RNA binding into the wider innate immune response. IFIT3 in humans, for example, is known to stimulate innate immune signalling by promoting the interaction between MAVS, an adaptor protein in the cytoplasm downstream of dsRNA sensing, and its activating kinase TBK1 (52, 53). The impact of a heterocomplex of IFIT1 and IFIT3, bound to non-self RNA, on innate immune signalling has yet to be investigated. IFIT3 additionally forms a heterocomplex with the proapoptotic IFIT2, via a different interaction interface in the N-terminus, and decreases IFIT2-directed cell death (14, 54). Therefore, in humans but not in mice, the regulation of IFIT1 is intrinsically linked to the regulation of IFIT2, since they share a cofactor. The implications of IFIT co-regulation in innate immunity, apoptosis and other cellular processes are still unknown.

In summary this present study, coupled with previous evolutionary analyses of the IFIT family (3, 4), has revealed convergent mechanisms for RNA binding and complex formation between species, even while the IFIT locus itself has undergone major restructuring. A model for convergent human IFIT and murine Ifit function is presented in Figure 10. In humans there is a single protein, IFIT1, which binds very strongly to non-self cap0-RNA, but may also weakly bind to self cap1-RNA, and inhibit their translation (4, 8, 11, 16). Human IFIT1 is highly expressed in response to IFN (12), along with its cofactor IFIT3, which promotes its stability and translation inhibition activity (13, 14). By contrast in mice, murine Ifit1 binds only to cap0-RNA and is highly expressed (16), while murine Ifit1b binds strongly to cap1-RNA but is poorly expressed

in stimulated mouse cells, as we have demonstrated here. Both proteins are regulated by Ifit1c, which acts as a cofactor analogous to human IFIT3. In this way, murine and human cells may achieve the same balance of cap0- and cap1-RNA binding during the IFN response. Therefore, considering the IFIT locus together, rather than examining individual genes, could be more valuable in examining IFIT molecular function.

Experimental procedures

Plasmids

Ifit promoter sequences were defined as 1 kb upstream of the annotated transcription start site for each Ifit gene, derived from their respective mRNA sequences (Ifit1: NM_008331.3, Ifit1b_1: NM_001362130.1, Ifit1b_2: NM_053217.2, Ifit1c: NM_001110517.1), except in the case of Ifit1b_2, where only 0.8 kb of sequence was included owing to highly repetitive DNA in the most distal 5′ sequence. Promoters were cloned between MluI and XhoI sites in pGL3 Basic (Promega), upstream of Firefly luciferase. pRL-TK (Promega) was included as a normalisation control.

For reporter RNA transcription, the firefly luciferase reporter gene flanked by the 5′ and 3′ UTRs of the MHV N protein subgenomic mRNA, which shares 5′ and 3′ terminal sequences with all MHV mRNAs (NC_001846.1) was synthesised with a 5′ T7 promoter sequence (IDT) and inserted between EcoRI and PstI sites in pUC57. pUC57-globin-Fluc (14) and pUC57-ZIKV-Fluc (55) were previously described.

For bacterial expression, sequences for murine Ifit1 (NP_032357.2), Ifit1b (NP_444447.1), Ifit1c (NP_001095075.1), Ifit2 (NP_032358.1), Ifit3 (NP_034631.1) and Ifit3b (NP_001005858.2) were inserted into pTriEx1.1 to contain a C-terminal 8xHis tag, as previously described (32). For MBP-tagged proteins, Ifit sequences were inserted between NdeI and BamHI sites in pOPTHM, which contains an N-terminal His6 tag followed by an MBP tag. pOPTHM-Ifit1c$_{CTD}$ was generated by PCR amplification of the C-terminal domain of Ifit1c and pOPTH-Ifit1c$_{CTD}$ was generated by overlapping PCR to remove the MBP tag. Mutants were derived from these plasmids by site directed mutagenesis PCR using overlapping primers. The plasmids for expression of human IFIT1 (10) and IFIT3 (14) have been described.

For mammalian cell expression, pCDNA3.1 containing Ifit sequences with an N-terminal FLAG tag were purchased from Genscript. For co-expression, eGFP was PCR amplified to contain a 5′ NheI site and Kozak sequence and 3′ NdeI and BamHI sites, followed by XbaI. This eGFP fragment was then inserted into pCDNA3.1 between NheI and XbaI sites. Ifit1 or Ifit1b was then inserted between the introduced NdeI and BamHI sites. Ifit1c was PCR amplified to contain a 5′ thosea asigna virus 2A sequence, followed by a FLAG tag. The 3′ end was WT or contained the YL mutation. The 5′ and 3′ sequences were engineered to overlap the regions flanking the pCDNA3.1-eGFP-Ifit1b BamHI site, to allow insertion by Gibson assembly. Since eGFP-Ifit1 did not express in mouse cells, pCDNA3.1-mCherry-Ifit1 was derived from pCDNA3.1-eGFP-Ifit1 by inserting the mCherry tag between NheI and EcoRI sites to replace the eGFP tag. Ifit1c was then inserted into the BamHI site by Gibson assembly, as previously. RNA binding mutants of Ifit1 (pCDNA3.1-mCherry-Ifit1WM) and Ifit1b (pCDNA3.1-eGFP-Ifit1bWM) were generated by site directed mutagenesis, producing W144M and W152M mutants, respectively.

Recombinant protein expression and purification

Recombinant proteins were expressed in Rosetta2 (DE3) pLysS *Escherichia coli* cells (Novagen). Cells were grown to an OD_{600} of 0.4-1 in 2x TY medium. Protein expression was induced using 1 mM isopropyl b-D-1-thiogalactopyranoside, at 20 °C for 20 hours. Cells were harvested and lysed in buffer containing 400 mM KCl, 40 mM Tris-HCl pH 7.5, 5% glycerol, 2 mM DTT, 0.5 mM PMSF and 1 mg/mL lysozyme. Proteins were isolated by affinity chromatography on Ni-NTA agarose resin (Qiagen) or PureCube 100 Ni-NTA agarose (Cube Biotech). Proteins were typically polished by FPLC on Superdex 200 increase 10/300 or HiLoad 16/600 columns (GE Healthcare), in Buffer I (200 mM KCl, 40 mM Tris-HCl pH 7.5, 5 % glycerol, 1 mM DTT), concentrated to > 1 mg/mL, then stored at -70 °C. Recombinant IFNβ was produced as previously described from HEK293T cells transfected with pCDNA3-IFN-β (56). Supernatant was harvested after 24 hours, aliquoted, and stored at -70 °C and was diluted 1:500 in cell culture media to stimulate cells.

***In vitro* transcription**

Plasmids were linearised with FspI (globin), PmlI (MHV) or HindIII (ZIKV), and purified by gel extraction (globin) or ethanol precipitation (MHV and ZIKV). RNA was transcribed from 0.5 – 2 μg linearised template using 50 ng/μL recombinant T7 RNA polymerase in transcription buffer (40 mM HEPES-NaOH pH 7.5, 32 mM MgOAc, 40 mM DTT, 2 mM spermidine, 10 mM ATP, 10 mM CTP, 10 mM GTP, 10 mM UTP, 0.2 U/μL RNaseOUT (Invitrogen)), for 2-4 hours at 37 °C. RNA was purified by DNaseI treatment, acidic phenol extraction and ethanol precipitation. Residual nucleotides were removed using Illustra MicroSpin G-50 columns (GE Healthcare). To produce cap0 and cap1 RNA, 40-60 μg RNA was capped using the ScripCap m7G capping system and 2′-O-methyltransferase system (CellScript). Cap2 RNA was generated from cap1 templates using 200 ng/μL recombinant cap2 methyltransferase in cap2 buffer (50 mM Tris-HCl pH 7.5, 5 mM DTT, 2 mM S-adenosyl methionine, 0.1 U/μL RNaseOUT), incubated at 20 ˚C for 4 hours before acidic phenol extraction and ethanol precipitation, as described above. Residual nucleotides and SAM were removed using Illustra MicroSpin G-50 columns (GE Healthcare).

Short RNA transcripts (5′-GACATTTGCTTCTGACACAACTGTG-3′) were transcribed from negative strand DNA oligonucleotide templates, containing a 3′ negative strand T7 promoter sequence (5′-CACAGTTGTGTCAGAAGCAAATGTCTATAGTGAGTCGTATTA-3′), annealed to a T7 promoter-containing forward primer (5′-TAATACGACTCACTATA-3′). RNA was transcribed from 5-10 μM annealed DNA oligos, in modified transcription buffer (500 ng/μL T7 polymerase, 40 mM HEPES-NaOH pH 7.5, 13.4 mM MgOAc, 40 mM DTT, 2 mM spermidine, 0.6 mM ATP, 4 mM CTP, 6 mM GTP, 0.6 mM UTP, and 0.1 U/μL RNaseOUT (Invitrogen)). After purification, to remove residual nucleotides, RNA was polished by FPLC on a HiLoad Superdex 75 pg 16/600 column (GE healthcare) in milliQ water at 4 °C, at a flow rate of 1 mL/min. Peak fractions were concentrated by ethanol precipitation. Up to 150 μg (~ 200 μM) oligonucleotide RNA was capped in modified capping reactions, containing 1 mM (cap0 reactions) or 2 mM (cap1 reactions) S-adenosyl methionine (NEB) and residual nucleotides were again removed by size exclusion.

Denaturing PAGE

Short RNAs were denatured by boiling for 5 minutes at 75 °C in 50% formamide loading buffer and separated in 15 % acrylamide 7 M urea gels (Bio-Rad Mini-PROTEAN format) at 300 V for 35 minutes. Longer RNAs were separated in 6 % acrylamide 7 M urea gels at 300 V for 45 minutes. Gels were stained in 1x TBE containing 2 μg/mL ethidium bromide for 10 minutes, then washed twice in water before imaging under 302 nm ultraviolet light.

Primer extension inhibition

For the 2′-O-methylation assay, 50 ng Cy5-labelled primer (Sigma) was annealed to 40 nM RNA by heating to 75 °C for 5 minutes and snap-cooling on ice. Reverse transcription was carried out using 5 U avian myoblastosis virus (AMV) reverse transcriptase (Promega) in 20 mM Tris-HCl pH 7.5, 100 mM KCl, 0.5 mM dNTPs with 0-4 mM MgOAc. For IFIT binding experiments, 25 ng Cy5-labelled primer was annealed to 10 nM RNA, then incubated with indicated concentrations of IFIT in 20 μL reactions containing 20 mM Tris-HCl pH 7.5, 100 mM KCl, 2.5 mM $MgCl_2$, 1 mM ATP, 0.2 mM GTP, 1 mM DTT, 0.25 mM spermidine, 0.1 U/μL RNaseOUT and 0.5 mg/mL bovine serum albumin (BSA). Reactions were incubated at 37 ˚C for 10 minutes before addition of 2.5 U AMV reverse transcriptase (Promega), 4 mM $MgCl_2$, 0.5 mM dNTPs and labelled primer, either Cy5 (Figure S8A) or ^{32}P (Perkin-Elmer) (Figure S8D). Reverse transcription reactions were incubated at 37 ˚C for 30 minutes, then stopped with 100 mM EDTA and 10% SDS. cDNA products were extracted with UltraPure phenol:chloroform:isoamylalcohol (25:24:1) pH 8 (ThermoFisher) and ethanol precipitated. Pellets were resuspended in 91 % formamide loading dye and boiled for 5 minutes at 75 °C for PAGE. cDNA products were separated by 6% denaturing PAGE on 35 cm sequencing gels for 30-60 minutes, then imaged directly on an FLA7000 Typhoon scanner (GE).

***In vitro* translation**

For translation inhibition assays, Ifit proteins were serially diluted in BSA buffer in a volume of 2.5 μL (20 mM Tris-HCl pH 7.5, 150 mM KCl, 5 % glycerol, 1 mM DTT, 0.5 mg/mL BSA, 10 U/μL RNaseOUT). 125 ng Fluc reporter RNA bearing different 5′ and 3′UTRs (15-20 nM final) was added to diluted Ifits and incubated at 30 ˚C for 15 minutes for RNA binding. *In vitro* translation was then carried out using the Flexi rabbit reticulocyte lysate (RRL) system (Promega) at 30 °C for 90 minutes. For murine Ifit complexes, 500 nM MBP-Ifit1c$_{CTD}$ or the equivalent volume of Buffer I was included in the RRL master mix. Reactions were incubated at 30 ˚C for 90 minutes, then stopped by addition of 50 μL passive lysis buffer (Promega) on ice. Stopped translation reactions were diluted 1:10 and an equal volume of firefly luciferase assay reagent was added, to a final volume of 50 μL. Luminescence was measured by GloMax for 10 seconds per well. Data were normalised to the no IFIT control for each experiment. 50% inhibitory concentrations (IC_{50}) were derived by fitting to [Inhibitor] versus normalised response curve $(Y = 100)/(1 + (X^{HillSlope})/(IC_{50}{}^{HillSlope}))$ using the least squares method in GraphPad Prism. Confidence intervals were calculated using the likelihood ratio asymmetric method and a replicates test was performed to test for lack of it. Curves were compared by extra sum of squares F-test.

Co-precipitation

For co-precipitation experiments, 2.5 μM MBP-tagged bait protein was incubated with 2.5 μM prey protein at 30 ˚C for 1 hour, in Buffer P (20 mM Tris-HCl pH 7.5, 200 mM KCl, 5 % glycerol, 0.1 % NP-40, 1 mM EDTA, 5 mM DTT) in a final volume of 40 μL. Proteins were centrifuged at 15,000g for 60 seconds to

remove any precipitate, then applied to equilibrated amylose magnetic beads (NEB) for 30 minutes, in a final volume of 200 µL. Beads were washed 3 times for one minute in Buffer P, then eluted by incubation for 20 minutes with 100 mM maltose in Buffer P. For competition assays, beads were washed once in Buffer P, followed by 3 washes with increasing concentrations of competitor protein (0.5, 1 and 2 µM), for 10 minutes each. Beads were washed once in Buffer P before elution. 10 µL samples were taken at each stage for SDS-PAGE analysis.

Differential scanning fluorimetry

To assay RNA binding, a dilution series of 25 nt model RNAs, up to 16 µM, were mixed with 2 µM protein and 1:500 Protein Thermal Shift dye in 20 mM HEPES-NaOH pH 7.5, 150 mM KCl, 5% glycerol, 1 mM DTT and 20 ng/µL yeast tRNA (Ambion). For testing the stability of IFIT proteins and complexes, in an optical 96-well reaction plate (Applied Biosystems), 2.5 µg protein was mixed with 1:500 Protein Thermal Shift dye (Life Technologies) in 20 mM HEPES-NaOH pH 7.5, 150 mM KCl, 2.5 mM MgOAc, 5% glycerol and 1 mM DTT, in a final volume of 20 µL. Emission was measured at 623 nm in a ViiA7 Real-Time PCR system (Applied Biosystems), ramping from 25 to 95 ˚C stepwise at a rate of 1 ˚C per 20S. For interpolation of melting temperatures, data were analysed using the Bolzmann equation ($y = LL + (UL - LL)/(1 + \exp(Tm - x)/1)$) where LL and UL are the minimum and maximum fluorescence intensities, respectively, and melting temperature (Tm) was interpolated from the 50% intersect of the curve.

Size-exclusion chromatography multi-angle light scattering

Ifit proteins (1 mg/mL) were analysed by size exclusion chromatography (SEC) on a Superdex 200 Increase 10/300 GL column at 4 ˚C at a flow rate of 0.5 mL/min. Ifit complexes were examined by combining Ifit proteins at stoichiometric concentrations for 1 hour at 4 ˚C or 30 ˚C, before SEC analysis. 280 nm absorbance was normalised such that peak height was equal to 1, for ease of comparison. For SEC-MALS, Ifit1b (0.5 or 2 mg/mL in a 150 µL loop) was applied to a Superdex 200 Increase 10/300 GL column at room temperature, at a flow rate of 0.4 mL/min. Multi-angle light scattering (MALS) analysis was performed by inline measurement of static light scattering (DAWN 8+, Wyatt Technology), differential refractive index (Optilan T-rEX, Wyatt Technology) and 280 nm absorbance (Aligent 1260 UV, Aligent Technologies). Molecular mass was calculated using the AS-TRA6 software package (Wyatt Technology). Access to SEC-MALS apparatus was kindly provided by Dr Janet Deane.

Cell lines

Human embryonic kidney (HEK293T), murine macrophage-like (RAW264.7) and murine embryonic fibroblast (MEF) cell lines all from ATCC were maintained in Dulbecco's modified Eagle's medium (DMEM) with 4.5 mg/mL glucose supplemented with 10% foetal calf serum, 2 mM L-glutamine, penicillin (100 SI units/mL) and streptomycin (100 µg/mL). Murine 17 clone 1 (17Cl-1) cells, derived from spontaneously transformed BALB/c 3T3 fibroblasts (30), kindly shared by Dr Nerea Irigoyen, were maintained in DMEM with 1 mg/mL glucose.

Transfection of mammalian cells

For Ifit induction experiments, cells were stimulated with 2 µg polyI:C (Sigma) transfected using Lipofectamine 2000 (Invitrogen). To determine Ifit promoter activity, 17Cl-1 cells were transfected at 70%

confluency with 800 ng pGL3-Ifit promoter plasmid and 200 ng pRL-TK, using Lipofectamine 2000. After 6 hours, cells were stimulated with 1:100 recombinant IFNβ (produced as described above). Cells were harvested after 24 hours by washing in PBS and lysis in passive lysis buffer (Promega). Promoter activity was measured using the Dual-Glo luciferase assay system (Promega) with a Glomax luminometer (Promega). Fluc signal was normalised to Rluc signal, and fold changes were calculated between IFN-treated and mock-treated wells. For puromycylation experiments, 17Cl-1 cells were transfected with 2 μg per well pCDNA3.1-FLAG-Ifit plasmids, or empty pCDNA3.1, using Lipofectamine 2000. After 16 hours, nascent proteins were labelled using puromycin at 5 μg/mL for 4 hours. Cells were harvested by washing in PBS and lysis in passive lysis buffer. Puromycin signal was detected by immunoblotting, as described below, and was quantified using ImageJ, normalised to the tubulin signal. For Ifit co-expression experiments, 17Cl-1 cells were seeded into 6 well plates containing glass coverslips. At 60% confluency, 2.5 pmol Ifit coexpression plasmids (described above) were transfected using Lipofectamine 2000. After 24 hours, coverslips were fixed and stained for immunofluorescence microscopy, as described below, and surrounding cells from the same well were harvested for immunoblotting using passive lysis buffer.

Electroporation of mammalian cells

For infection experiments, transfection using Lipofectamine 2000 inhibited infection, therefore plasmids were transfected by electroporation. $1x10^6$ 17Cl-1 cells were mixed with 2.5 pmol Ifit coexpression plasmids (described above) in 100 μL Opti-MEM (Gibco), in a 2 mm electroporation cuvette. Cells were electroporated using a NEPA21 electroporator (Nepagene) at 125V for 7.5 seconds. Cells were seeded subconfluently into 24 well plates with glass coverslips, or into T25 flasks, and left to recover for 18 hours before infection.

Virus culture

Recombinant mouse hepatitis virus strain A59 (MHV-A59) was a gift from Dr Nerea Irigoyen, derived from a full-length cDNA clone, as described (57, 58). 18 hours after plasmid electroporation, cells were infected at a multiplicity of infection (MOI) of 0.1 or 5 PFU/cell in low glucose DMEM containing 50 μg/mL DEAE-dextran and 0.2% BSA. After 45 minutes at 37 ˚C, inoculum was removed and replaced with fresh media. After 14 hours, cells on coverslips were fixed and stained for immunofluorescence microscopy and cells in T25 flasks were trypsinised, fixed and stained in suspension for flow cytometry analysis (described below).

Quantitative PCR

qPCR primers were designed to detect Ifit1b, Ifit1c, Ifit2, Ifit3 and Ifit3b, within the coding sequence of the second exon (Table S1). Primers for Ifit1 have been described (59). End-point PCR was performed using Taq polymerase (Invitrogen) on 10 ng pTriEx1.1-Ifit template plasmid to verify primer specificity. RNA was extracted from cell lysates in passive lysis buffer, using TRI reagent (Sigma) and cDNA was generated using Moloney murine leukemia virus reverse transcriptase (Promega) and random hexamer primers. qPCR was performed using the qPCR core kit for SYBR green I with low ROX passive reference (Eurogentec), with the manufacturer's recommended parameters: 95 ˚C for 15 seconds then 60 ˚C for 1 minute, for 50 cycles. Data were normalised against GAPDH and expressed as fold change over mock (2-ddCq).

To verify linear amplification, 10-fold serial dilutions of linearised Ifit plasmid were made from 100 ng (1.5×10^{10} copies) to 10 ag (1.5 copies) of DNA per well and qPCR was performed as described above. Linear regression was performed on CT values plotted against $\log_{10}$-transformed DNA mass, to ensure PCR efficiency was within acceptable parameters (90-110%). To verify target specificity, qPCR products amplified from IFN-treated RAW264.7 cells were purified by gel extraction, and Sanger sequenced.

SDS-PAGE and immunoblotting

Proteins were resolved by 12.5% SDS-PAGE. Where similarly-sized proteins were difficult to resolve, proteins were separated on precast 4-12 % NuPAGE Bis-Tris gels (Invitrogen) in MES buffer (Invitrogen) (co-precipitation experiments, Figure 6), at 180V for 110 minutes at 4 °C. Gels were stained using coomassie brilliant blue R, destained in 25% ethanol and imaged using a LiCor Odyssey imaging system. For immunoblotting, separated proteins were transferred to 0.45 μm nitrocellulose membrane. Membranes were probed with anti-Ifit1 (sc-134949, Santa Cruz, 1:500), anti-IFIT1 (PA3-848, Pierce, 1:500; cross-reactive with murine Ifit1 and Ifit1b), anti-IFIT2 (12604-1-AP, Proteintech, 1:800; cross-reactive against murine Ifit2 and Ifit3/3b), anti-GAPDH (AM4300, Invitrogen, 1:8000), anti-tubulin (ab6160, Abcam, 1:1000), anti-His (34660, Qiagen, 1:1000), anti-FLAG M2-peroxidase (A8592, Sigma, 1:1000), anti-GFP (G1544, Sigma, 1:4000) and anti-mCherry (ab213511 Abcam, 1:1000). The mouse monoclonal antibody against puromycin was a kind gift from Prof Ian Goodfellow. Rat polyclonal antibodies against Ifit1b and Ifit1c were raised and purified by Eurogentec. Ifit1b antiserum was raised against CFQMKKATSRENRKRA and ESHKSHIHDSLDELRC peptides and affinity purified against ESHKSHIHDSLDELRC. Ifit1c antiserum was raised against CKASNMQPRGEDRKRA and CEKHIEETLPRISSQP peptides and affinity purified against CEKHIEETLPRISSQP. Membranes were then probed with IRdye secondary antibodies (Li-Cor) and imaged on an Odyssey CLx Imaging System (Li-Cor). For puromycylation experiments, to visualise total protein, membranes were stained using REVERT (Li-Cor), then destained, before blocking.

Immunofluorescence microscopy

Cells were fixed in 3% paraformaldehyde in PBS, then permeabilised in 0.1% Triton X-100 in PBS with 50 mM NH_4Cl. Cells were blocked in PBS with 0.2% fish gelatine, 0.02% NaN_3 and 0.01% Triton X-100. Coverslips were stained with anti-FLAG (F1804, Sigma, 1:1000) and anti-dsRNA (10010500, SCIONS English and Scientific consulting, 1:1000) with Alexa Fluor secondary antibodies (Life Technologies), before mounting using ProLong Gold Antifade Reagent with 4′,6-diamidino-2-phenulindole (DAPI) (Invitrogen). Slides were visualised using either the 10x objective (Figure 4B) or the 60x oil immersion objective (Figure 8D,E) of an Olympus IX81 wide field microscope, using Image Pro Plus software. Merged pseudocoloured images were generated in ImageJ.

Flow cytometry

Murine 17Cl-1 cells were electroporated with Ifit expression plasmids, as described above, then seeded into T25 flasks. After 24 hours, cells (~2.5×10^6) were infected with MHV A59 at an MOI of 0.05 pfu/cell. After 16 hours, cells were harvested by trypsinisation, followed by fixation in 1% paraformaldehyde and permeabilisation in ice-cold methanol. Cells were blocked with 2% FCS in PBS, before staining with anti-

dsRNA (10010500, SCIONS English and Scientific consulting, 1:600) and Alexa Fluor secondary antibodies (Life Technologies), before analysis on an Attune NxT flow cytometer (Invitrogen). Data were analysed using FlowJo (v. 10.6.2).

Graphs and statistics

Graphs were generated in GraphPad Prism (v. 7.03) or Microsoft Excel (Micrsosoft Office 2013, Version 15.0.5119.1000). For pairwise comparisons of data means throughout, data were analysed by two-tailed Student's t-test, assuming unequal variance, as indicated in the figure legends. Nonlinear regression was carried out using GraphPad Prism, as described above.

Structural modelling

RNA secondary structural models and free energy calculations were generated with Mfold (60). Protein homology models were generated using SWISS-MODEL (61), based on known IFIT structures as indicated in the relevant figure legends. Protein structures were visualised using the PyMOL Molecular Graphics System (Version 1.5.0.5, Schrödinger, LLC, www.pymol.org). Structures and models for Figure 9 were visualised using Illustrate (62).

Phylogenetic analysis

Mammalian IFIT mRNA sequences were assembled by Daugherty et al. *(2016)*. Protein sequences were aligned using MUSCLE (63) and maximum likelihood trees were built and visualised in Seaview (64) using PhyML (65), with 100 bootstrap replicates for statistical support. Sequence alignments of IFIT3 proteins in different species were visualised using CIAlign (https://pypi.org/project/cialign/) (66).

Data availability

All data are contained within the manuscript and online Supporting Information.

Acknowledgements

The authors are grateful to Nerea Irygoyen and Ian Goodfellow for sharing reagents, to Janet Deane for access to equipment and to Katherine Brown for help with the CIAlign tool.

Funding and additional information

This work was funded by a Royal Society/Wellcome Trust Sir Henry Dale Fellowship (202471/Z/16/Z to TRS). HVM was supported by a University of Cambridge, Department of Pathology PhD Studentship.

Conflict of interest

The authors declare that they have no conflicts of interest with the contents of this article.

References

1. Cowling, V. H. (2010) Regulation of mRNA cap methylation. *Biochem. J.* **425**, 295–302
2. Decroly, E., Ferron, F., Lescar, J., and Canard, B. (2012) Conventional and unconventional mechanisms for capping viral mRNA. *Nat. Rev. Microbiol.* **10**, 51–65
3. Liu, Y., Zhang, Y.-B., Liu, T.-K., and Gui, J.-F. (2013) Lineage-Specific Expansion of IFIT Gene Family: An Insight into Coevolution with IFN Gene Family. *PLoS One*. **8**, e66859
4. Daugherty, M. D., Schaller, A. M., Geballe, A. P., and Malik, H. S. (2016) Evolution-guided functional analyses reveal diverse antiviral specificities encoded by IFIT1 genes in mammals. *Elife*. **5**, 1–22
5. Yang, Z., Liang, H., Zhou, Q., Li, Y., Chen, H., Ye, W., Chen, D., Fleming, J., Shu, H., and Liu, Y. (2012) Crystal structure of ISG54 reveals a novel RNA binding structure and potential functional mechanisms. *Cell Res.* **22**, 1328–1338
6. Feng, F., Yuan, L., Wang, Y. E., Crowley, C., Lv, Z., Li, J., Liu, Y., Cheng, G., Zeng, S., and Liang, H. (2013) Crystal structure and nucleotide selectivity of human IFIT5/ISG58. *Cell Res.* **23**, 1055–8
7. Abbas, Y. M., Pichlmair, A., Górna, M. W., Superti-Furga, G., and Nagar, B. (2013) Structural basis for viral 5′-PPP-RNA recognition by human IFIT proteins. *Nature*. **494**, 60–4
8. Abbas, Y. M., Laudenbach, B. T., Martínez-Montero, S., Cencic, R., Habjan, M., Pichlmair, A., Damha, M. J., Pelletier, J., and Nagar, B. (2017) Structure of human IFIT1 with capped RNA reveals adaptable mRNA binding and mechanisms for sensing N1 and N2 ribose 2′-O methylations. *Proc. Natl. Acad. Sci.* **114**, E2106–E2115
9. Katibah, G. E., Qin, Y., Sidote, D. J., Yao, J., Lambowitz, A. M., and Collins, K. (2014) Broad and adaptable RNA structure recognition by the human interferon-induced tetratricopeptide repeat protein IFIT5. *Proc. Natl. Acad. Sci.* **111**, 12025–12030
10. Katibah, G. E., Lee, H. J., Huizar, J. P., Vogan, J. M., Alber, T., and Collins, K. (2013) tRNA binding, structure, and localization of the human interferon-induced protein IFIT5. *Mol. Cell*. **49**, 743–50
11. Kumar, P., Sweeney, T. R., Skabkin, M. a, Skabkina, O. V, Hellen, C. U. T., and Pestova, T. V (2014) Inhibition of translation by IFIT family members is determined by their ability to interact selectively with the 5′-terminal regions of cap0-, cap1- and 5′ppp- mRNAs. *Nucleic Acids Res.* **42**, 3228–3245
12. Pichlmair, A., Lassnig, C., Eberle, C.-A., Górna, M. W., Baumann, C. L., Burkard, T. R., Bürckstümmer, T., Stefanovic, A., Krieger, S., Bennett, K. L., Rülicke, T., Weber, F., Colinge, J., Müller, M., and Superti-Furga, G. (2011) IFIT1 is an antiviral protein that recognizes 5′-triphosphate RNA. *Nat. Immunol.* **12**, 624–630
13. Johnson, B., VanBlargan, L. A., Xu, W., White, J. P., Shan, C., Shi, P.-Y., Zhang, R., Adhikari, J., Gross, M. L., Leung, D. W., Diamond, M. S., and Amarasinghe, G. K. (2018) Human IFIT3 Modulates IFIT1 RNA Binding Specificity and Protein Stability. *Immunity*. **48**, 487-499.e5
14. Fleith, R. C., Mears, H. V, Leong, X. Y., Sanford, T. J., Emmott, E., Graham, S. C., Mansur, D. S., and Sweeney, T. R. (2018) IFIT3 and IFIT2/3 promote IFIT1-mediated translation inhibition by enhancing binding to non-self RNA. *Nucleic Acids Res.* **46**, 5269–5285
15. Mears, H. V, and Sweeney, T. R. (2018) Better together: the role of IFIT protein-protein interactions in the antiviral response. *J. Gen. Virol.* **99**, 1463–1477
16. Habjan, M., Hubel, P., Lacerda, L., Benda, C., Holze, C., Eberl, C. H., Mann, A., Kindler, E., Gil-Cruz, C., Ziebuhr, J., Thiel, V., and Pichlmair, A. (2013) Sequestration by IFIT1 Impairs Translation of 2′O-unmethylated Capped RNA. *PLoS Pathog.* **9**, e1003663
17. Daffis, S., Szretter, K. J., Schriewer, J., Li, J., Youn, S., Errett, J., Lin, T.-Y. Y., Schneller, S., Zust, R., Dong, H., Thiel, V., Sen, G. C., Fensterl, V., Klimstra, W. B., Pierson, T. C., et al. (2010) 2′-O methylation of the viral mRNA cap evades host restriction by IFIT family members. *Nature*. **468**, 452–456
18. Szretter, K. J., Daniels, B. P., Cho, H., Gainey, M. D., Yokoyama, W. M., Gale, M., Virgin, H.

W., Klein, R. S., Sen, G. C., and Diamond, M. S. (2012) 2′-O methylation of the viral mRNA cap by West Nile virus evades ifit1-dependent and -independent mechanisms of host restriction in vivo. *PLoS Pathog.* **8**, e1002698

19. Li, S.-H., Dong, H., Li, X.-F., Xie, X., Zhao, H., Deng, Y.-Q., Wang, X.-Y., Ye, Q., Zhu, S.-Y., Wang, H.-J., Zhang, B., Leng, Q.-B., Zuest, R., Qin, E.-D., Qin, C.-F., et al. (2013) Rational Design of a Flavivirus Vaccine by Abolishing Viral RNA 2′-O Methylation. *J. Virol.* **87**, 5812–5819
20. Züst, R., Dong, H., Li, X.-F., Chang, D. C., Zhang, B., Balakrishnan, T., Toh, Y.-X., Jiang, T., Li, S.-H., Deng, Y.-Q., Ellis, B. R., Ellis, E. M., Poidinger, M., Zolezzi, F., Qin, C.-F., et al. (2013) Rational Design of a Live Attenuated Dengue Vaccine: 2′-O-Methyltransferase Mutants Are Highly Attenuated and Immunogenic in Mice and Macaques. *PLoS Pathog.* **9**, e1003521
21. Menachery, V. D., Gralinski, L. E., Mitchell, H. D., Dinnon, K. H., Leist, S. R., Yount, B. L., Graham, R. L., McAnarney, E. T., Stratton, K. G., Cockrell, A. S., Debbink, K., Sims, A. C., Waters, K. M., and Baric, R. S. (2017) Middle East Respiratory Syndrome Coronavirus Nonstructural Protein 16 Is Necessary for Interferon Resistance and Viral Pathogenesis. *mSphere*. **2**, e00346-17
22. Menachery, V. D., Yount, B. L., Josset, L., Gralinski, L. E., Scobey, T., Agnihothram, S., Katze, M. G., and Baric, R. S. (2014) Attenuation and restoration of severe acute respiratory syndrome coronavirus mutant lacking 2′-O-methyltransferase activity. *J. Virol.* **88**, 4251–64
23. Züst, R., Cervantes-Barragan, L., Habjan, M., Maier, R., Neuman, B. W., Ziebuhr, J., Szretter, K. J., Baker, S. C., Barchet, W., Diamond, M. S., Siddell, S. G., Ludewig, B., and Thiel, V. (2011) Ribose 2′-O-methylation provides a molecular signature for the distinction of self and non-self mRNA dependent on the RNA sensor Mda5. *Nat. Immunol.* **12**, 137–143
24. Bluyssen, H. A., Vlietstra, R. J., van der Made, A., and Trapman, J. (1994) The interferon-stimulated gene 54 K promoter contains two adjacent functional interferon-stimulated response elements of different strength, which act synergistically for maximal interferon-alpha inducibility. *Eur. J. Biochem.* **220**, 395–402
25. Smith, J. B., and Herschman, H. R. (1996) The glucocorticoid attenuated response genes GARG-16, GARG-39, and GARG-49/IRG2 encode inducible proteins containing multiple tetratricopeptide repeat domains. *Arch. Biochem. Biophys.* **330**, 290–300
26. Terenzi, F., Pal, S., and Sen, G. C. (2005) Induction and mode of action of the viral stress-inducible murine proteins, P56 and P54. *Virology*. **340**, 116–124
27. Terenzi, F., White, C., Pal, S., Williams, B. R. G., and Sen, G. C. (2007) Tissue-Specific and Inducer-Specific Differential Induction of ISG56 and ISG54 in Mice. *J. Virol.* **81**, 8656–8665
28. Zamudio, J. R., Mittra, B., Campbell, D. A., and Sturm, N. R. (2009) Hypermethylated cap 4 maximizes Trypanosoma brucei translation. *Mol. Microbiol.* **72**, 1100–1110
29. Zamudio, J. R., Mittra, B., Zeiner, G. M., Feder, M., Bujnicki, J. M., Sturm, N. R., and Campbell, D. A. (2006) Complete Cap 4 Formation Is Not Required for Viability in Trypanosoma brucei. *Eukaryot. Cell*. **5**, 905–915
30. Sturman, L. S., and Takemoto, K. K. (1972) Enhanced growth of a murine coronavirus in transformed mouse cells. *Infect. Immun.* **6**, 501–7
31. Weber, F., Wagner, V., Rasmussen, S. B., Hartmann, R., and Paludan, S. R. (2006) Double-stranded RNA is produced by positive-strand RNA viruses and DNA viruses but not in detectable amounts by negative-strand RNA viruses. *J. Virol.* **80**, 5059–64
32. Mears, H. V., Emmott, E., Chaudhry, Y., Hosmillo, M., Goodfellow, I. G., and Sweeney, T. R. (2019) Ifit1 regulates norovirus infection and enhances the interferon response in murine macrophage-like cells. *Wellcome Open Res.* **4**, 82
33. Cook, G., Brown, K., Franaszek, K., Moore, N., Siddell, S., Brierley, I., Firth, A., and Irigoyen, N. (2018) Probing the unfolded protein response to mouse hepatitis coronavirus infection through RNA sequencing and ribosome profiling. *bioRxiv*. 10.1101/292979
34. Perry, R. P., and Kelley, D. E. (1976) Kinetics of formation of 5′ terminal caps in mRNA. *Cell*. **8**,

433–442
35. Wang, J., Alvin Chew, B. L., Lai, Y., Dong, H., Xu, L., Balamkundu, S., Cai, W. M., Cui, L., Liu, C. F., Fu, X.-Y., Lin, Z., Shi, P.-Y., Lu, T. K., Luo, D., Jaffrey, S. R., et al. (2019) Quantifying the RNA cap epitranscriptome reveals novel caps in cellular and viral RNA. *Nucleic Acids Res.* 10.1093/nar/gkz751
36. Schmidt, E. K., Clavarino, G., Ceppi, M., and Pierre, P. (2009) SUnSET, a nonradioactive method to monitor protein synthesis. *Nat. Methods*. **6**, 275–277
37. Semisotnov, G. V., Rodionova, N. A., Razgulyaev, O. I., Uversky, V. N., Gripas', A. F., and Gilmanshin, R. I. (1991) Study of the "molten globule" intermediate state in protein folding by a hydrophobic fluorescent probe. *Biopolymers*. **31**, 119–128
38. Niesen, F. H., Berglund, H., and Vedadi, M. (2007) The use of differential scanning fluorimetry to detect ligand interactions that promote protein stability. *Nat. Protoc.* **2**, 2212–2221
39. Abbas, Y. M., Martínez-montero, S., Cencic, R., Pelletier, J., and Peter, D. (2017) A conserved homo-dimerization interface in human IFIT1 provides insights into IFIT interactome assembly. *bioRxiv*. https://doi.org/10.1101/152850
40. Liu, Z., Chen, O., Wall, J. B. J., Zheng, M., Zhou, Y., Wang, L., Ruth Vaseghi, H., Qian, L., and Liu, J. (2017) Systematic comparison of 2A peptides for cloning multi-genes in a polycistronic vector. *Sci. Rep.* **7**, 2193
41. Guo, J., Peters, K. L., and Sen, G. C. (2000) Induction of the human protein P56 by interferon, double-stranded RNA, or virus infection. *Virology*. **267**, 209–219
42. Huang, X., Shen, N., Bao, C., Gu, Y., Wu, L., and Chen, S. (2008) Interferon-induced protein IFIT4 is associated with systemic lupus erythematosus and promotes differentiation of monocytes into dendritic cell-like cells. *Arthritis Res. Ther.* **10**, 1–12
43. Fensterl, V., and Sen, G. C. (2015) Interferon-Induced Ifit Proteins: Their Role in Viral Pathogenesis. *J. Virol.* **89**, 2462–2468
44. Pidugu, V. K., Pidugu, H. B., Wu, M. M., Liu, C. J., and Lee, T. C. (2019) Emerging Functions of Human IFIT Proteins in Cancer. *Front. Mol. Biosci.* **6**, 1–16
45. Butchi, N. B., Hinton, D. R., Stohlman, S. A., Kapil, P., Fensterl, V., Sen, G. C., and Bergmann, C. C. (2014) Ifit2 Deficiency Results in Uncontrolled Neurotropic Coronavirus Replication and Enhanced Encephalitis via Impaired Alpha/Beta Interferon Induction in Macrophages. *J. Virol.* **88**, 1051–1064
46. Reolon, L. W., Vichier-Guerre, S., de Matos, B. M., Dugué, L., Assunção, T. R. da S., Zanchin, N. I. T., Pochet, S., and Guimarães, B. G. (2019) Crystal structure of the Trypanosoma cruzi EIF4E5 translation factor homologue in complex with mRNA cap-4. *Nucleic Acids Res.* **47**, 5973–5987
47. Hyde, J. L., Gardner, C. L., Kimura, T., White, J. P., Liu, G., Trobaugh, D. W., Huang, C., Tonelli, M., Paessler, S., Takeda, K., Klimstra, W. B., Amarasinghe, G. K., and Diamond, M. S. (2014) A viral RNA structural element alters host recognition of nonself RNA. *Science.* **343**, 783–7
48. Reynaud, J. M., Kim, D. Y., Atasheva, S., Rasalouskaya, A., White, J. P., Diamond, M. S., Weaver, S. C., Frolova, E. I., and Frolov, I. (2015) IFIT1 Differentially Interferes with Translation and Replication of Alphavirus Genomes and Promotes Induction of Type I Interferon. *PLoS Pathog.* **11**, e1004863
49. Gebhard, L. G., Filomatori, C. V., and Gamarnik, A. V. (2011) Functional RNA elements in the dengue virus genome. *Viruses*. **3**, 1739–56
50. Wacher, C., Muller, M., Hofer, M. J., Getts, D. R., Zabaras, R., Ousman, S. S., Terenzi, F., Sen, G. C., King, N. J. C., and Campbell, I. L. (2007) Coordinated Regulation and Widespread Cellular Expression of Interferon-Stimulated Genes (ISG) ISG-49, ISG-54, and ISG-56 in the Central Nervous System after Infection with Distinct Viruses. *J. Virol.* **81**, 860–871
51. Guo, J., Hui, D. J., Merrick, W. C., and Sen, G. C. (2000) A new pathway of translational regulation mediated by eukaryotic initiation factor 3. *EMBO J.* **19**, 6891–9
52. Liu, X.-Y. X.-Y., Chen, W., Wei, B. B., Shan, Y.-F., and Wang, C. (2011) IFN-Induced TPR

Protein IFIT3 Potentiates Antiviral Signaling by Bridging MAVS and TBK1. *J. Immunol.* **187**, 2559–2568
53. Hou, Z., Zhang, J., Han, Q., Su, C., Qu, J., Xu, D., Zhang, C., and Tian, Z. (2016) Hepatitis B virus inhibits intrinsic RIG-I and RIG-G immune signaling via inducing miR146a. *Sci. Rep.* **6**, 26150
54. Stawowczyk, M., Van Scoy, S., Kumar, K. P., and Reich, N. C. (2011) The interferon stimulated gene 54 promotes apoptosis. *J. Biol. Chem.* **286**, 7257–66
55. Chavali, P. L., Stojic, L., Meredith, L. W., Joseph, N., Nahorski, M. S., Sanford, T. J., Sweeney, T. R., Krishna, B. A., Hosmillo, M., Firth, A. E., Bayliss, R., Marcelis, C. L., Lindsay, S., Goodfellow, I., Woods, C. G., et al. (2017) Neurodevelopmental protein Musashi-1 interacts with the Zika genome and promotes viral replication. *Science*. **357**, 83–88
56. van Pesch, V., Lanaya, H., Renauld, J.-C., and Michiels, T. (2004) Characterization of the Murine Alpha Interferon Gene Family. *J. Virol.* **78**, 8219–8228
57. Coley, S. E., Lavi, E., Sawicki, S. G., Fu, L., Schelle, B., Karl, N., Siddell, S. G., and Thiel, V. (2005) Recombinant Mouse Hepatitis Virus Strain A59 from Cloned, Full-Length cDNA Replicates to High Titers In Vitro and Is Fully Pathogenic In Vivo. *J. Virol.* **79**, 3097–3106
58. Irigoyen, N., Firth, A. E., Jones, J. D., Chung, B. Y. W., Siddell, S. G., and Brierley, I. (2016) High-Resolution Analysis of Coronavirus Gene Expression by RNA Sequencing and Ribosome Profiling. *PLoS Pathog.* **12**, e1005473
59. Tamassia, N., Le Moigne, V., Rossato, M., Donini, M., McCartney, S., Calzetti, F., Colonna, M., Bazzoni, F., and Cassatella, M. A. (2008) Activation of an Immunoregulatory and Antiviral Gene Expression Program in Poly(I:C)-Transfected Human Neutrophils. *J. Immunol.* **181**, 6563–6573
60. Zuker, M. (2003) Mfold web server for nucleic acid folding and hybridization prediction. *Nucleic Acids Res.* **31**, 3406–3415
61. Waterhouse, A., Bertoni, M., Bienert, S., Studer, G., Tauriello, G., Gumienny, R., Heer, F. T., De Beer, T. A. P., Rempfer, C., Bordoli, L., Lepore, R., and Schwede, T. (2018) SWISS-MODEL: Homology modelling of protein structures and complexes. *Nucleic Acids Res.* **46**, W296–W303
62. Goodsell, D. S., Autin, L., and Olson, A. J. (2019) Illustrate: Software for Biomolecular Illustration. *Structure*. **27**, 1716-1720.e1
63. Edgar, R. C. (2004) MUSCLE: multiple sequence alignment with high accuracy and high throughput. *Nucleic Acids Res.* **32**, 1792–7
64. Gouy, M., Guindon, S., and Gascuel, O. (2010) SeaView version 4: A multiplatform graphical user interface for sequence alignment and phylogenetic tree building. *Mol. Biol. Evol.* **27**, 221–4
65. Guindon, S., Dufayard, J.-F., Lefort, V., Anisimova, M., Hordijk, W., and Gascuel, O. (2010) New algorithms and methods to estimate maximum-likelihood phylogenies: assessing the performance of PhyML 3.0. *Syst. Biol.* **59**, 307–21
66. Tumescheit, C., Firth, A. E., and Brown, K. (2020) CIAlign - A highly customisable command line tool to clean , interpret and visualise multiple sequence alignments . *bioRxiv*. https://doi.org/10.1101/2020.09.14.291484

Figure 1. Induction of Ifit gene expression in stimulated murine cells.
(**A**) Genome organisation of the murine Ifit locus. Exons are shown as boxes with arrows indicating the direction of the reading frame, and introns as solid black lines. Black asterisks represent canonical interferon-stimulated response elements (ISRE) while grey stars indicate putative ISRE-like sequences. For Ifit1b, two transcription start sites are annotated. (**B-C**) RT-qPCR analysis of RNA extracted from (B) RAW264.7 cells or (C) 17Cl-1 cells stimulated with IFNβ or transfected with polyI:C over 48 hours. Graphs show the mean and standard error of two biological replicates. (**D-E**) Immunoblot analysis of (D) RAW264.7 or (E) 17Cl-1 cell lysates extracted at the same time as (C/D). GAPDH is included as a loading control for each membrane. See also Figure S1-S4.

Figure 2. Translation inhibition by murine Ifit proteins.
(**A**) Schematic of the mRNA 5′ cap. (**B**) Schematic of the Globin-Fluc mRNA, showing the primer binding site for reverse transcription (upper panel) and primer extension analysis of capped Globin-Fluc mRNAs at different concentrations, to analyse cap methylation efficiency (lower panel). At lower Mg^{2+} concentrations, additional stops are visible corresponding to 2′-O-methylation of the first and second nucleotides, indicated with arrowheads. At high Mg^{2+} concentrations an additional band is seen at the -1 position, consistent with terminal transferase activity of the reverse transcriptase. (**C**) SDS-PAGE (upper panel) and anti-His (lower panel) western blot of recombinant Ifit proteins. (**D**) *In vitro* translation of differentially capped Globin-Fluc reporter mRNAs, normalised to the BSA-only control. Graphs show the mean and the standard error of at least three experiments. Data were compared to the BSA-only control by pairwise two-tailed t-tests and p values < 0.1 are shown.

Figure 3. Ifit1b inhibits translation of unstructured cap1-RNA.
(**A**) Schematics of reporter mRNAs used for *in vitro* translation. (**B-D**) *In vitro* translation of differentially capped (B) Globin-Fluc, (C) MHV-Fluc or (D) ZIKV-Fluc, in RRL with increasing concentrations of Ifit1b, alongside titrations of Ifit1 on cap0 RNA for comparison (dashed lines). Data were normalised to the BSA-only control and shown as the mean and the standard error of at least two independent experiments. IC_{50} values are listed in Table 1.

Figure 4. Overexpression of Ifit1b inhibits MHV infection.
(**A**) Schematics of the MHV genome and experimental design. 17Cl-1 cells were electroporated with eGFP, eGFP-Ifit1b, mCherry-Ifit1 or empty vector (EV) 24 hours before infection with MHV strain A59 at an MOI of 0.01 pfu/cell. 12 or 14 hours after infection, cells were fixed on coverslips for immunofluorescence microscopy or fixed in suspension for flow cytometry analysis, as indicated. Cells were stained for double-stranded RNA (dsRNA) as a marker for viral replication. (**B**) Immunofluorescence and bright-field microscopy of mock or MHV-infected cells. Fluorescently-tagged Ifit proteins are shown in green, dsRNA is shown in magenta, and DAPI-stained nuclei are shown in blue. White arrowheads highlight cells which are positive for GFP or mCherry-Ifit1 as well as dsRNA, while open arrowheads highlight cells expressing eGFP-Ifit1b which are dsRNA-negative. (**C**) Flow cytometry analysis of mock (dashed lines) or MHV-infected (solid lines with shading) cells transfected with GFP (grey), GFP-Ifit1b (green) or GFP-Ifit1b-WM, an RNA-binding mutant (black). The black vertical line indicates the gate for dsRNA-positive cells on the x-axis. Quantification from this gate is shown in the lower panel. Data represent the mean and

standard deviation from two independent experiments. Data were compared by pairwise, two-tailed t-tests assuming unequal variance and p values <0.1 are shown. See also Figure S5-S7.

Figure 5. RNA binding by Ifit1b.
(**A**) Secondary structure prediction of the first 25 nt of the β-globin 5′UTR (globin25) RNA, calculated in Mfold (Zuker, 2003). (**B**) Denaturing PAGE analysis of uncapped, cap0 and cap1 globin25 RNA. (**C-D**) Thermal stability analysis of Ifit1 or Ifit1b with increasing concentrations of cap0 (grey) or cap1 (red) globin25 RNA. Quantification is shown in the left panels, expressed as the increase in melting temperature (Tm) over protein alone (dTm) (mean ± standard error from two-three independent experiments) and representative melt curves are shown in the right panels. Tm's were derived by non-linear regression using the Boltzmann equation, y = LL (UL – LL)/(1 + exp(Tm –x)/a) where LL and UL are lower limit and upper limit respectively. See also Figure S8.

Figure 6. Mutational analysis of Ifit1b RNA binding.
(**A**) Cartoon representation of the cap binding pocket of human IFIT1 (PDB: 5W5H), coloured by subdomain (SD). Bound cap0 oligo-A RNA is shown as black and orange sticks. Residues involved in human IFIT1 cap coordination and triphosphate binding are shown as sticks and labelled in black. The equivalent residues in murine Ifit1b, where divergent, are listed in red. (**B**) Coomassie-stained SDS-PAGE (upper panel) and anti-His western blot (lower panel) of wildtype (WT) and mutant Ifit1b. (**C**) Thermal shift assay of 2 μM WT and mutant Ifit1b with 4 μM cap0 or cap1 RNA, showing the difference in melting temperature (dTm) between protein only and protein with RNA. Graph shows the mean and standard deviation of three (cap0) or two (cap1) experimental replicates. (**D**) A model of Ifit1b (cyan) was generated in SWISS-MODEL, based on the structure of human IFIT1 (PDB: 5W5H), and is shown superposed with human IFIT1 (yellow). (Left panel) Residues in the cap-binding loop, distal to the 2′-O-hydroxyl group of the first RNA nucleotide, which impact cap0/cap1 binding specificity are shown as sticks. (Right panel) Residues proximal to the first RNA nucleotide are shown. In murine Ifit1b, a number of mutations (relative to IFIT1) are present in this region, which may allow accommodation of 2′-O-methylated/cap1-RNA.

Figure 7. Murine Ifit heterocomplex formation.
(**A**) Sequence alignment, showing the conserved YxxxL interaction motif (red box), which mediates interaction between human IFIT1 and IFIT3 (uppercase labels), and its conservation in murine Ifit proteins (lowercase labels). (**B-D**) Co-precipitation of Ifit1, Ifit1b and truncated Ifit1c (Ifit1c$_{CTD}$). MBP-tagged bait, or MBP alone, was incubated with prey proteins (lane 1) before binding to amylose resin. Unbound proteins were washed away (lanes 2-5) and bound proteins remained on the beads (lane 6). Bound proteins were eluted in maltose-containing buffer (lane 7). Ifit3 was included as a negative control in each experiment. (**E-G**) Thermal stability analysis of Ifit proteins and complexes. In (F,G), brighter shades of red indicate higher concentrations of Ifit1c$_{CTD}$. See also Figure S9-S12 and Table 2.

Figure 8. Heterocomplexing enhances murine Ifit stability in mouse cells.
(**A**) Schematics of Ifit coexpression plasmids. FP, fluorescent protein (mCherry or eGFP); T2A, thosea asigna virus 2A Stop-Go sequence. The Ifit1c sequence was either wildtype (WT) or contained mutations in the C-terminal domain to disrupt binding to Ifit1 or Ifit1b (Y456E/L460E, YL). (**B-E**) 17Cl-1 cells were

transfected with control or Ifit expression plasmids for 24 hours, then (B,C) harvested for immunoblotting or (D,E) stained for immunofluorescence. In (B,C), quantification of FLAG signal, normalised to GAPDH, is shown below each lane. Data represent the mean and standard deviation of two biological repeats. For consistency and visual clarity in (D,E), micrographs have been pseudocoloured such that fluorescent proteins (both mCherry and eGFP) are shown in green and anti-FLAG signal is shown in magenta. Micrographs are representative of at least two independent experiments. See also Figure S13.

Figure 9. Ifit1c enhances translation inhibition by Ifit1 and Ifit1b.
(**A**) Schematics of reporter mRNAs used for *in vitro* translation. (**B-D**) *In vitro* translation of MHV-Fluc reporter mRNAs in RRL with increasing concentrations of (B) Ifit1, (C) Ifit1b or (D) human IFIT1, in the presence or absence of 500 nM Ifit1c$_{CTD}$, either wildtype (WT) or YxxxL mutant (YL). Data were normalised to luciferase activity in the absence of IFIT protein, shown as the mean and standard error of at least two independent experiments. See Table 3 for calculated IC_{50} values.

Figure 10. Model for human IFIT and mouse Ifit function.
During an antiviral response in humans, IFIT1 is highly expressed following IFN stimulation. Human IFIT1 binds strongly to cap0-RNA (red) but weakly to cap1-RNA (blue), and inhibits their translation. Cap0-RNA is associated with viral infection and is recognised as 'non-self', while cellular RNA is typically cap1 modified and is therefore recognised as 'self'. As such, IFIT1 strongly inhibits the translation of 'non-self' viral RNA while only weakly inhibiting 'self' cellular RNA. In stimulated mouse cells, murine Ifit1 is strongly expressed and binds to cap0-RNA, while murine Ifit1b is poorly expressed and binds strongly to cap1-RNA. In this way, murine Ifit1 and Ifit1b acting together can strongly inhibit the translation of 'non-self' viral RNA while weakly inhibiting 'self' cellular RNA.
Human IFIT1 stability and activity is regulated by human IFIT3, which interacts via a conserved C-terminal interaction motif. Human IFIT3 also interacts with human IFIT2, via the N-terminus, and regulates IFIT2-mediated apoptosis. As such the human IFIT1:IFIT2:IFIT3 complex is co-regulated and is involved in multiple stages of the antiviral response. Murine Ifit1 and Ifit1b are both regulated by murine Ifit1c, which also interacts via the C-terminal domain. Ifit1, Ifit1b and Ifit1c do not bind to Ifit3, therefore the functions of Ifit heterocomplexes in mice are regulated separately.

Table 1. Translation inhibition by murine Ifit proteins.

Values are from data presented in Figure 3. IC_{50} values are the concentrations of Ifit that reduce reporter translation by 50% ± standard error. Data were fitted to [Inhibitor] versus normalized response curve ($Y = 100/(1 + (X^{HillSlope})/(IC_{50}{}^{HillSlope})$ using the least squares method in GraphPad Prism.

Ifit	RNA	IC_{50} (nM Ifit in RRL)
Ifit1b	cap0-globin-Fluc	675 ± 129
Ifit1b	cap1-globin-Fluc	152 ± 18.1
Ifit1b	cap2-globin-Fluc	826 ± 183
Ifit1	cap0-globin-Fluc	102 ± 14.5
Ifit1b	cap0-MHV-Fluc	690 ± 233
Ifit1b	cap1-MHV-Fluc	101 ± 17.9
Ifit1b	cap2-MHV-Fluc	238 ± 50.1
Ifit1	cap0-MHV-Fluc	68 ± 9.5
Ifit1b	cap1-ZIKV-Fluc	1240 ± 300
Ifit1	cap0-ZIKV-Fluc	550 ± 240

Table 2. Melting temperatures of Ifit proteins and complexes.

Melting temperatures (Tm) were interpolated from data presented in Figure 6. Data were analysed by non-linear regression using the Boltzmann equation, y = LL (UL – LL)/(1 + exp(Tm –x)/a) where LL and UL are lower limit and upper limit respectively.

Protein or complex	Tm (°C)
Ifit1	41.9
Ifit1b	38.3
Ifit1 + Ifit1c$_{CTD}$	44.4
Ifit1b + Ifit1c$_{CTD}$	41.0
MBP	57.7

Table 3. Translation inhibition by Ifit complexes.

Values are from data presented in Figure 9. IC_{50} values are the concentrations of Ifit that reduce reporter translation by 50% ± standard error. Data were fitted to [Inhibitor] versus normalized response curve ($Y = 100/(1 + (X^{HillSlope})/(IC_{50}{}^{HillSlope})$ using the least squares method in GraphPad Prism. *Curves were compared by extra sum-of-squares F test.

Ifit or complex	**RNA**	**IC_{50} (nM Ifit in RRL)**	**P-value (Ifit only vs complex)***
Ifit1b	cap1-MHV-Fluc	147 ± 27.8	-
Ifit1b + MBP-Ifit1c$_{CTD}$ WT	cap1-MHV-Fluc	32.6 ± 11.2	<0.0001
Ifit1b + MBP-Ifit1c$_{CTD}$ YL	cap1-MHV-Fluc	191 ± 28.4	0.6630
Ifit1	cap0-MHV-Fluc	67.9 ± 9.0	-
Ifit1 + MBP-Ifit1c$_{CTD}$ WT	cap0-MHV-Fluc	11.4 ± 5.8	<0.0001
Ifit1 + MBP-Ifit1c$_{CTD}$ YL	cap0-MHV-Fluc	68.7 ± 17.4	0.0577
IFIT1	cap0-MHV-Fluc	49.8 ± 7.3	-
IFIT1 + MBP-Ifit1c$_{CTD}$ WT	cap0-MHV-Fluc	55.0 ± 7.1	0.5044

Figure 1.

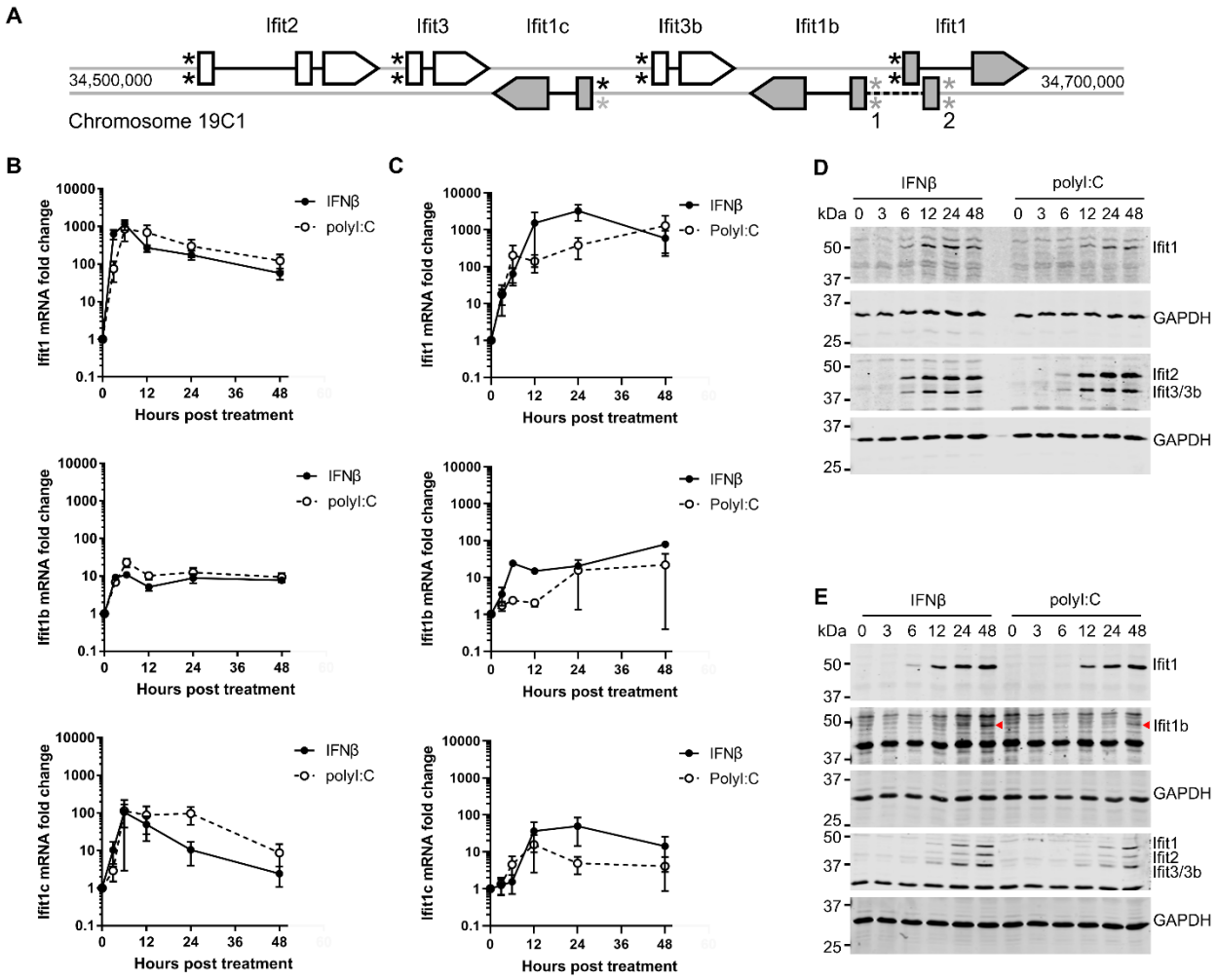
A
Ifit2
Ifit3
Ifit1c
Ifit3b
Ifit1b
Ifit1
34,500,000
34,700,000
Chromosome 19C1
1
2
B
C
Ifit1 mRNA fold change
Ifit1b mRNA fold change
Ifit1c mRNA fold change
IFNβ
polyI:C
PolyI:C
Hours post treatment
D
kDa 0 3 6 12 24 48 0 3 6 12 24 48
Ifit1
GAPDH
Ifit2
Ifit3/3b
E
Ifit1b
Ifit1
Ifit2
Ifit3/3b

Figure 2.

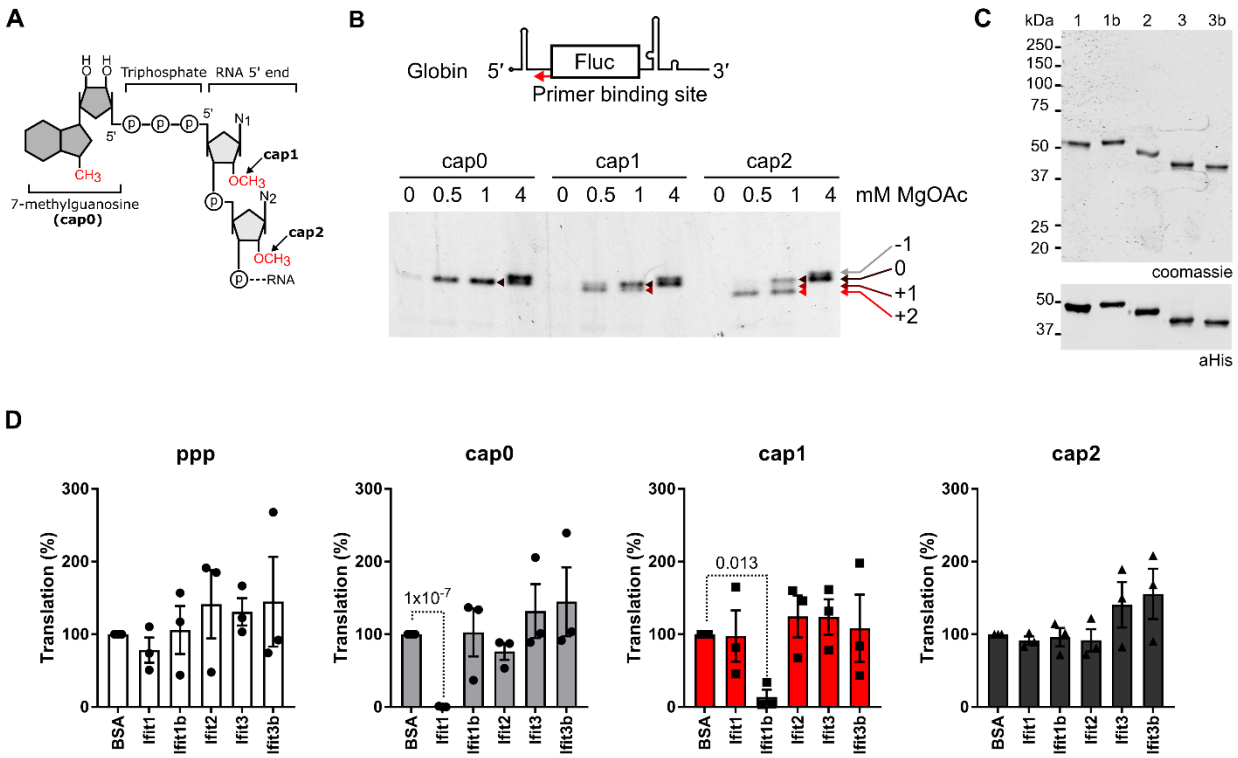
A
Triphosphate
RNA 5' end
7-methylguanosine
(cap0)
cap1
cap2
RNA
B
Globin
Fluc
Primer binding site
cap0
cap1
cap2
0 0.5 1 4 0 0.5 1 4 0 0.5 1 4 mM MgOAc
-1
0
+1
+2
C
kDa 1 1b 2 3 3b
250
150
100
75
50
37
25
20
coomassie
aHis
D
ppp
cap0
cap1
cap2
Translation (%)
1x10-7
0.013
BSA
Ifit1
Ifit1b
Ifit2
Ifit3
Ifit3b

Figure 3.

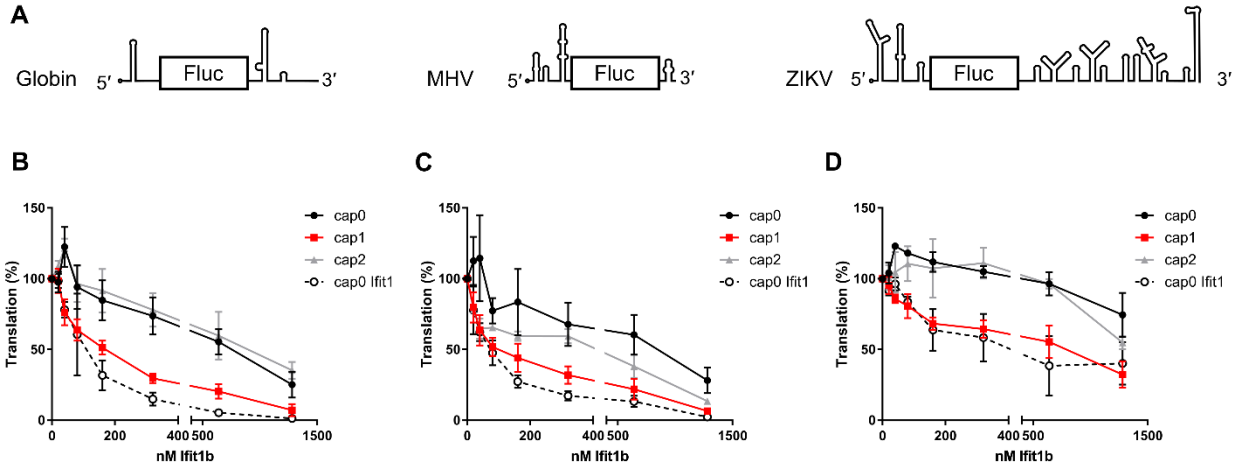
A
Globin
5′
Fluc
3′
MHV
5′
Fluc
3′
ZIKV
5′
Fluc
3′
B
C
D
Translation (%)
nM Ifit1b
cap0
cap1
cap2
cap0 Ifit1
0
50
100
150
200
400
500
1500

Figure 4.

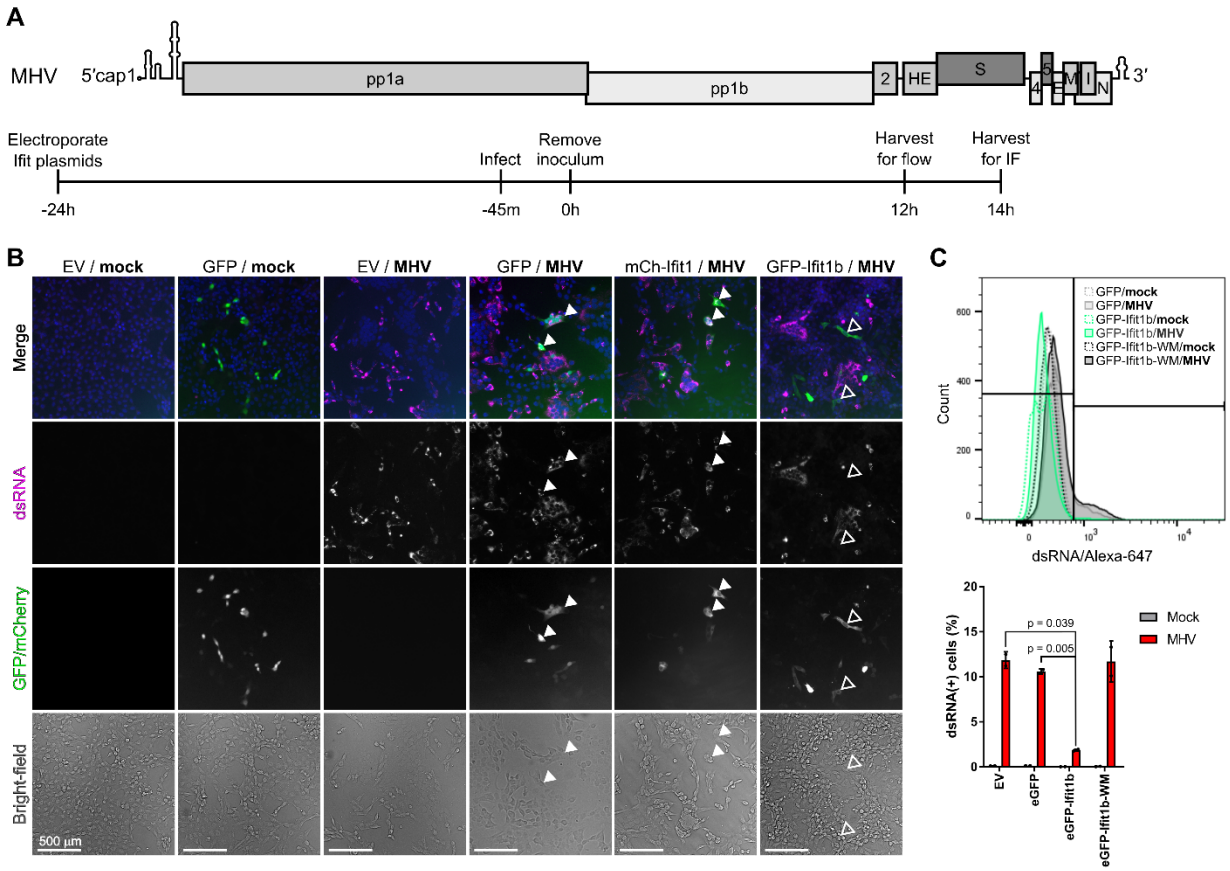
A
MHV
5'cap1
pp1a
pp1b
2
HE
S
4
5
M
I
N
3'
Electroporate Ifit plasmids
Infect
Remove inoculum
Harvest for flow
Harvest for IF
-24h
-45m
0h
12h
14h
B
EV / mock
GFP / mock
EV / MHV
GFP / MHV
mCh-Ifit1 / MHV
GFP-Ifit1b / MHV
Merge
dsRNA
GFP/mCherry
Bright-field
500 µm
C
GFP/mock
GFP/MHV
GFP-Ifit1b/mock
GFP-Ifit1b/MHV
GFP-Ifit1b-WM/mock
GFP-Ifit1b-WM/MHV
Count
dsRNA/Alexa-647
dsRNA(+) cells (%)
p = 0.039
p = 0.005
Mock
MHV
EV
eGFP
eGFP-Ifit1b
eGFP-Ifit1b-WM

Figure 5.

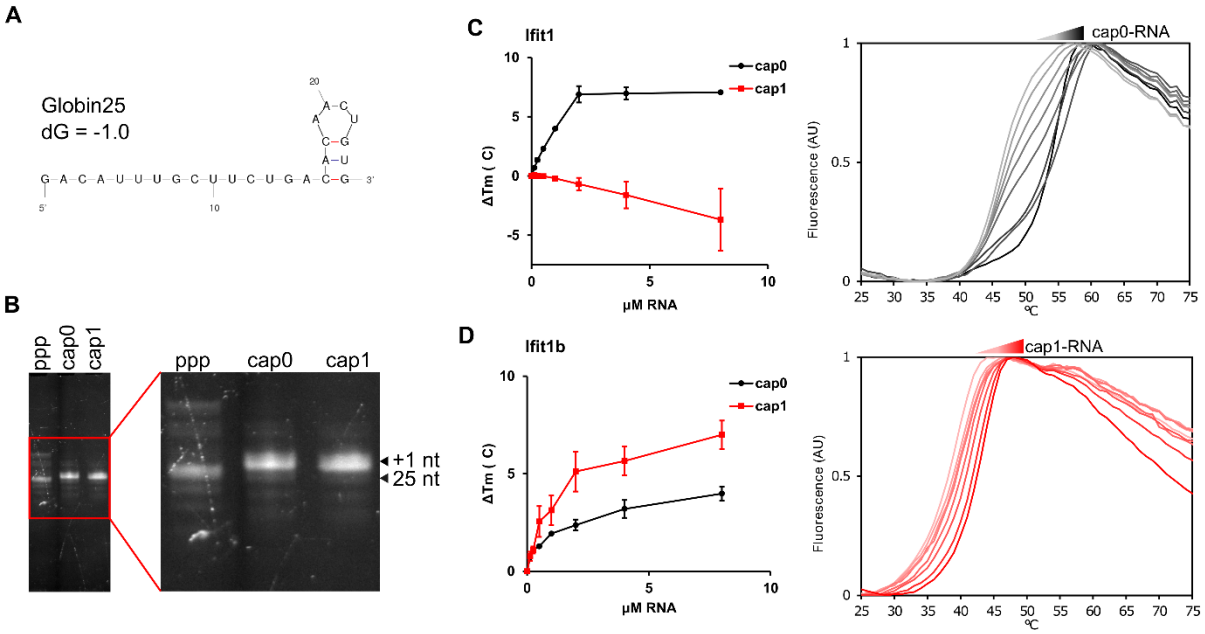
A
Globin25
dG = -1.0
G A C A U U U G C U U C U G A C G
5'
10
20
3'
B
ppp
cap0
cap1
ppp
cap0
cap1
+1 nt
25 nt
C
Ifit1
cap0
cap1
ΔTm (C)
μM RNA
cap0-RNA
Fluorescence (AU)
℃
D
Ifit1b
cap0
cap1
ΔTm (C)
μM RNA
cap1-RNA
Fluorescence (AU)
℃

Figure 6.

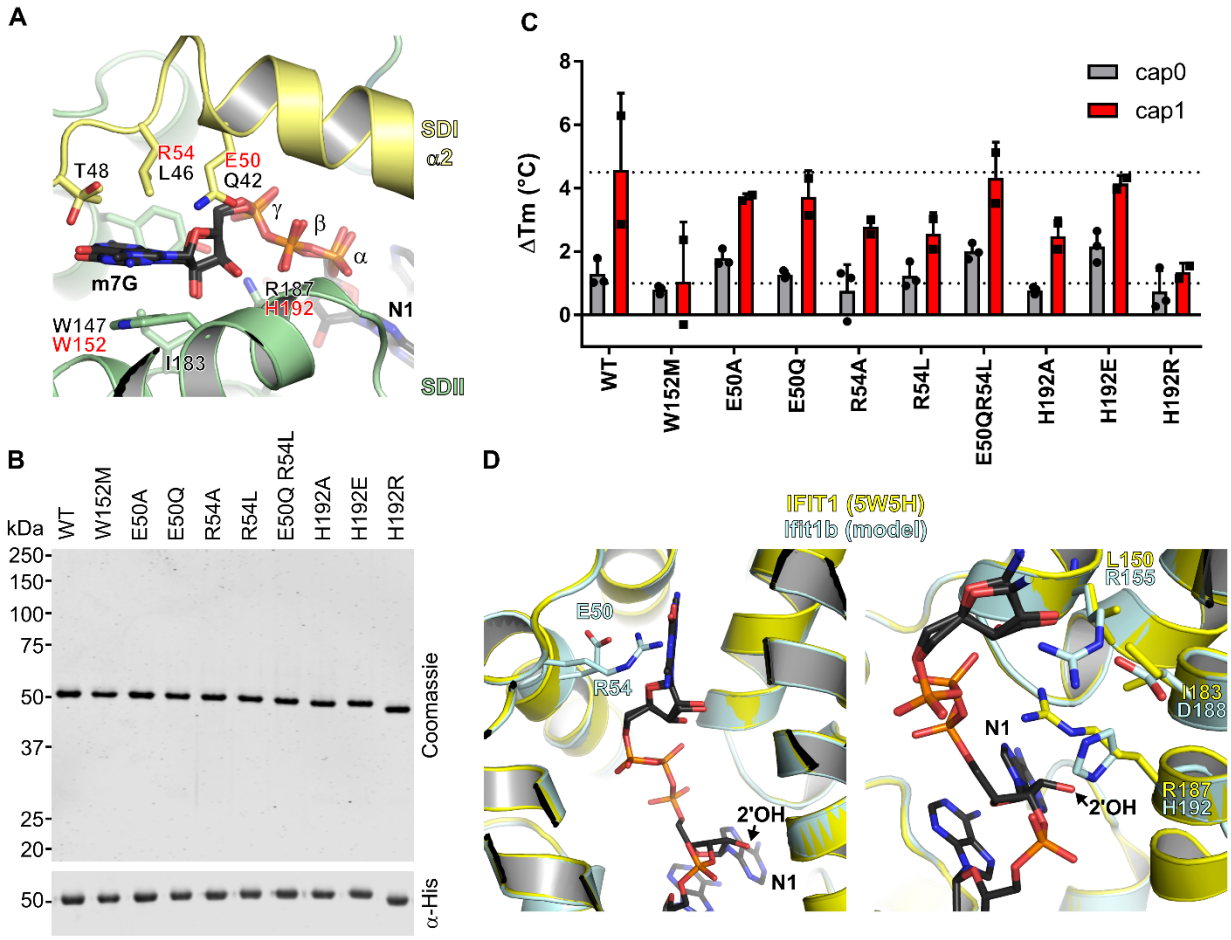
A
SDI
α2
R54
L46
E50
Q42
T48
γ
β
α
m7G
R187
H192
N1
W147
W152
I183
SDII
B
kDa
WT
W152M
E50A
E50Q
R54A
R54L
E50Q R54L
H192A
H192E
H192R
250-
150-
100-
75-
50-
37-
25-
20-
Coomassie
50-
α-His
C
cap0
cap1
ΔTm (°C)
8
6
4
2
0
WT
W152M
E50A
E50Q
R54A
R54L
E50QR54L
H192A
H192E
H192R
D
IFIT1 (5W5H)
Ifit1b (model)
E50
R54
2'OH
N1
L150
R155
I183
D188
N1
2'OH
R187
H192

Figure 7.

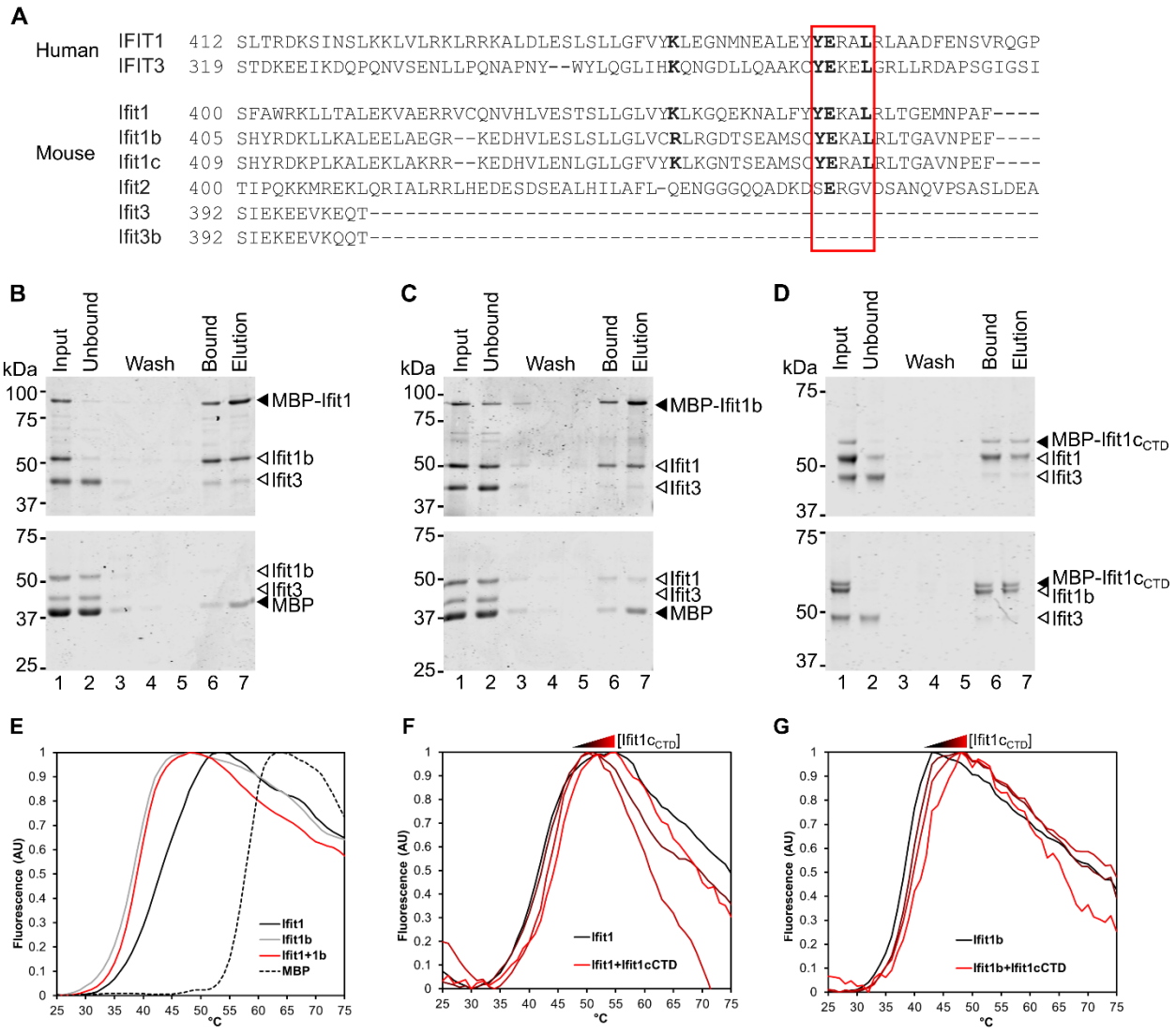
A
Human
IFIT1 412 SLTRDKSINSLKKLVLRKLRRKALDLESLSLLGFVYKLEGNMNEALEYYERALRLAADFENSVRQGP
IFIT3 319 STDKEEIKDQPQNVSENLLPQNAPNY--WYLQGLIHKQNGDLLQAAKCYEKELGRLLRDAPSGIGSI
Mouse
Ifit1 400 SFAWRKLLTALEKVAERRVCQNVHLVESTSLLGLVYKLKGQEKNALFYYEKALRLTGEMNPAF----
Ifit1b 405 SHYRDKLLKALEELAEGR--KEDHVLESLSLLGLVCRLRGDTSEAMSCYEKALRLTGAVNPEF----
Ifit1c 409 SHYRDKPLKALEKLAKRR--KEDHVLENLGLLGFVYKLKGNTSEAMSCYERALRLTGAVNPEF----
Ifit2 400 TIPQKKMREKLQRIALRRLHEDESDSEALHILAFL-QENGGGQQADKDSERGVDSANQVPSASLDEA
Ifit3 392 SIEKEEVKEQT----------
Ifit3b 392 SIEKEEVKQQT----------
B
kDa
Input
Unbound
Wash
Bound
Elution
MBP-Ifit1
Ifit1b
Ifit3
MBP
C
MBP-Ifit1b
Ifit1
Ifit3
MBP
D
MBP-Ifit1c$_{CTD}$
Ifit1
Ifit3
Ifit1b
E
Fluorescence (AU)
°C
Ifit1
Ifit1b
Ifit1+1b
MBP
F
[Ifit1c$_{CTD}$]
Ifit1
Ifit1+Ifit1cCTD
G
Ifit1b
Ifit1b+Ifit1cCTD

Figure 8.

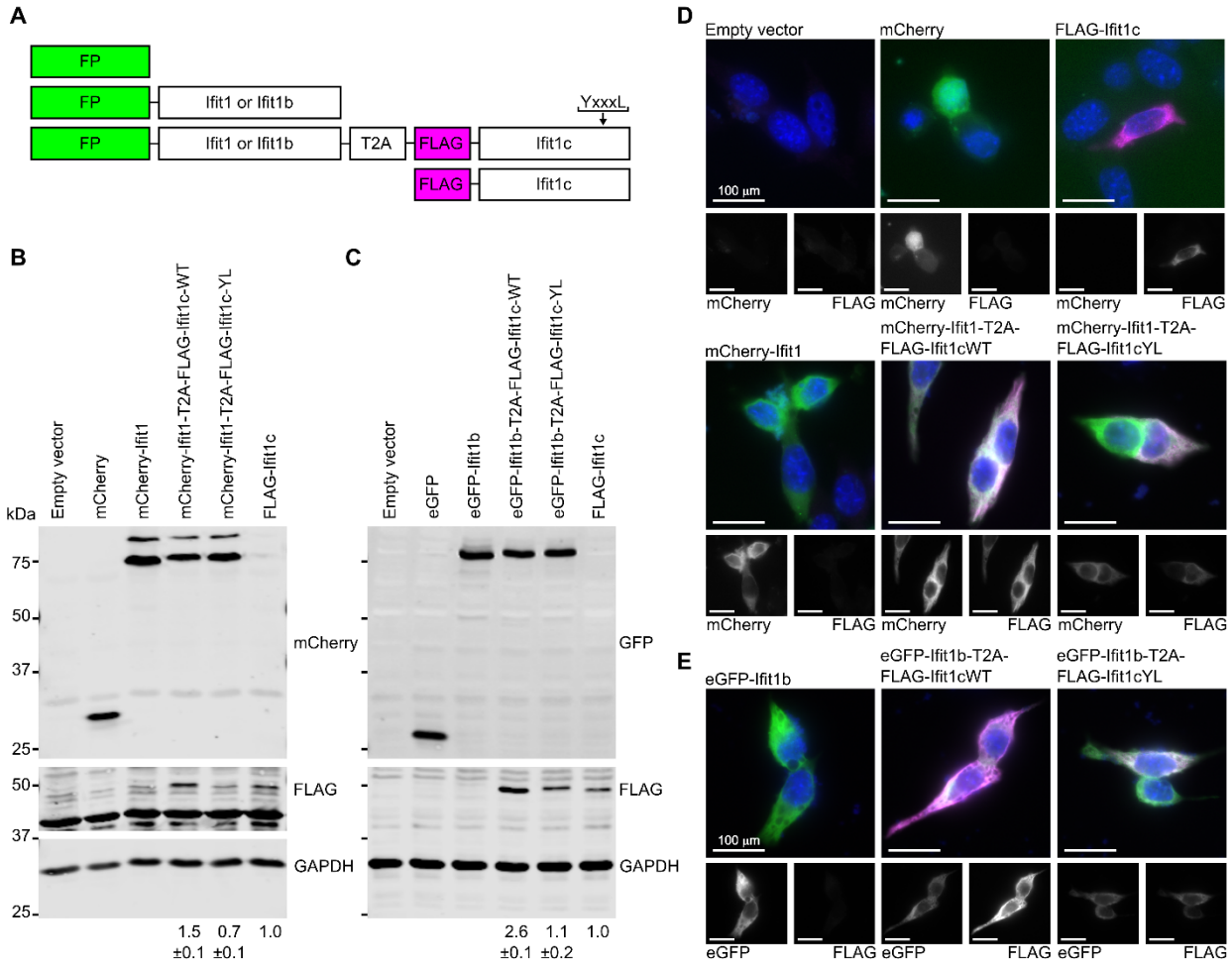
A
FP
FP
Ifit1 or Ifit1b
YxxxL
FP
Ifit1 or Ifit1b
T2A
FLAG
Ifit1c
FLAG
Ifit1c
B
kDa
Empty vector
mCherry
mCherry-Ifit1
mCherry-Ifit1-T2A-FLAG-Ifit1c-WT
mCherry-Ifit1-T2A-FLAG-Ifit1c-YL
FLAG-Ifit1c
75
50
37
25
mCherry
50
37
FLAG
GAPDH
25
1.5 ±0.1
0.7 ±0.1
1.0
C
Empty vector
eGFP
eGFP-Ifit1b
eGFP-Ifit1b-T2A-FLAG-Ifit1c-WT
eGFP-Ifit1b-T2A-FLAG-Ifit1c-YL
FLAG-Ifit1c
GFP
FLAG
GAPDH
2.6 ±0.1
1.1 ±0.2
1.0
D
Empty vector
mCherry
FLAG-Ifit1c
100 μm
mCherry
FLAG
mCherry
FLAG
mCherry
FLAG
mCherry-Ifit1
mCherry-Ifit1-T2A-FLAG-Ifit1cWT
mCherry-Ifit1-T2A-FLAG-Ifit1cYL
mCherry
FLAG
mCherry
FLAG
mCherry
FLAG
E
eGFP-Ifit1b
eGFP-Ifit1b-T2A-FLAG-Ifit1cWT
eGFP-Ifit1b-T2A-FLAG-Ifit1cYL
100 μm
eGFP
FLAG
eGFP
FLAG
eGFP
FLAG

Figure 9.

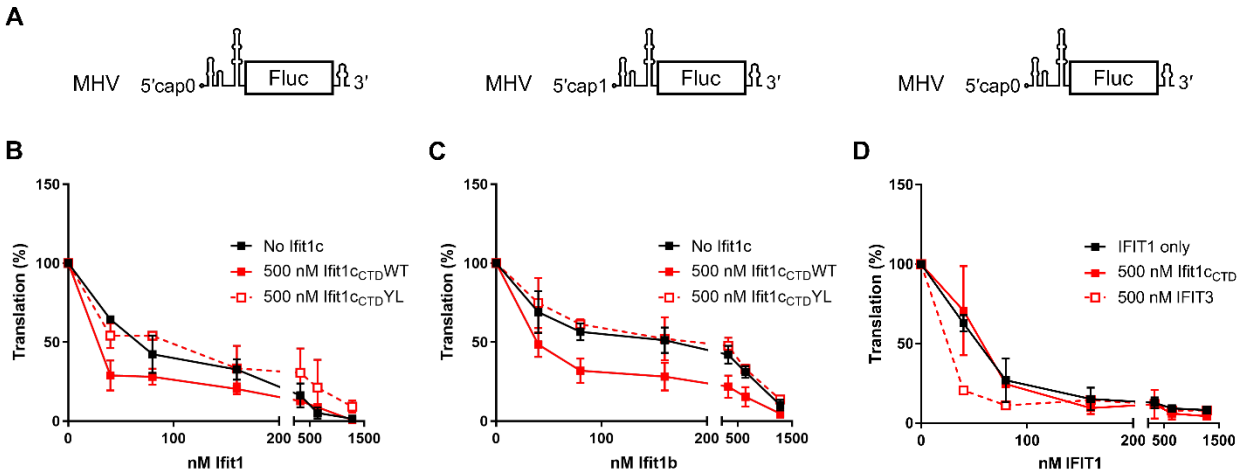
A
MHV 5′cap0 Fluc 3′
MHV 5′cap1 Fluc 3′
MHV 5′cap0 Fluc 3′
B
C
D
Translation (%)
No Ifit1c
500 nM Ifit1c$_{CTD}$WT
500 nM Ifit1c$_{CTD}$YL
nM Ifit1
nM Ifit1b
IFIT1 only
500 nM Ifit1c$_{CTD}$
500 nM IFIT3
nM IFIT1

Figure 10.

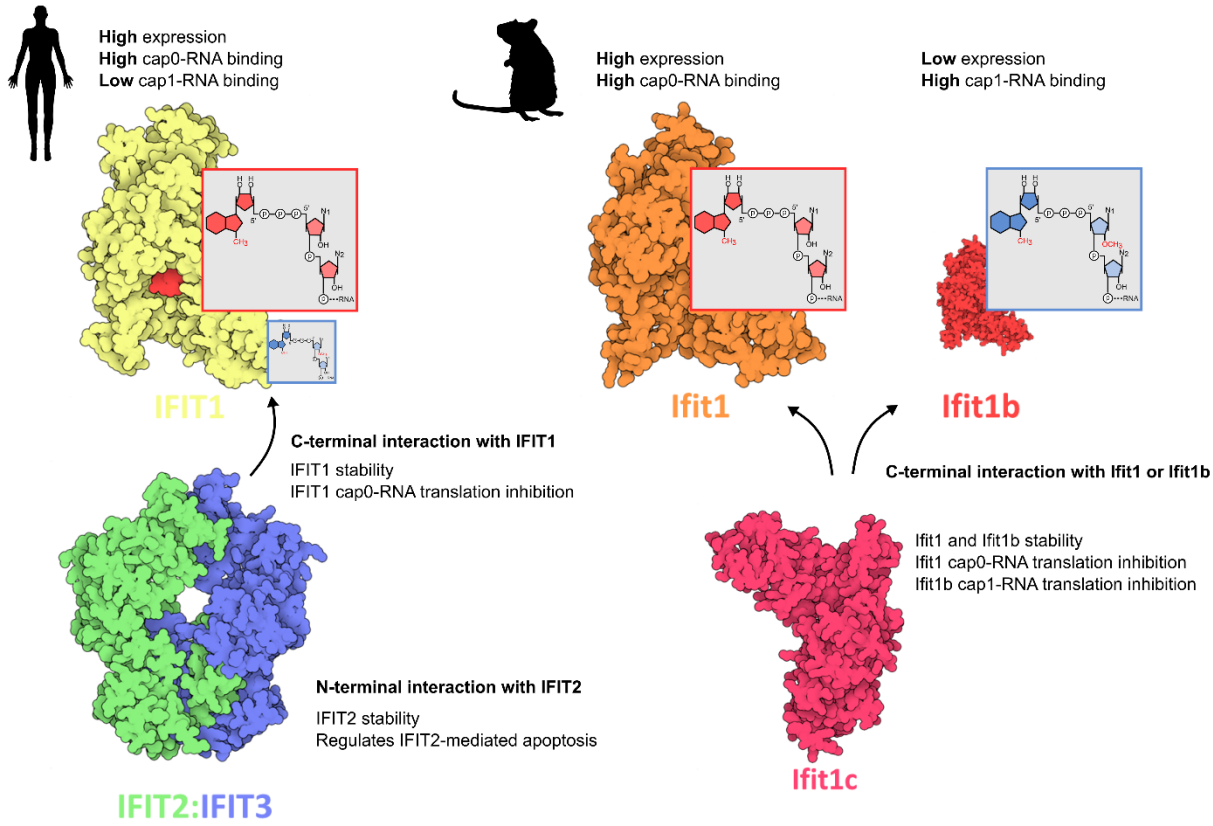
High expression
High cap0-RNA binding
Low cap1-RNA binding
IFIT1
C-terminal interaction with IFIT1
IFIT1 stability
IFIT1 cap0-RNA translation inhibition
IFIT2:IFIT3
N-terminal interaction with IFIT2
IFIT2 stability
Regulates IFIT2-mediated apoptosis
High expression
High cap0-RNA binding
Ifit1
Low expression
High cap1-RNA binding
Ifit1b
C-terminal interaction with Ifit1 or Ifit1b
Ifit1 and Ifit1b stability
Ifit1 cap0-RNA translation inhibition
Ifit1b cap1-RNA translation inhibition
Ifit1c